

Impact of Low-Level Jets on the Nocturnal Urban Heat Island Intensity in Oklahoma City

XIAO-MING HU

Center for Analysis and Prediction of Storms, University of Oklahoma, Norman, Oklahoma

PETRA M. KLEIN AND MING XUE

Center for Analysis and Prediction of Storms and School of Meteorology, University of Oklahoma, Norman, Oklahoma

JULIE K. LUNDQUIST

Department of Atmospheric and Oceanic Sciences/Renewable and Sustainable Energy Institute, University of Colorado, Boulder, Colorado

FUQING ZHANG

Department of Meteorology, The Pennsylvania State University, University Park, Pennsylvania

YOU CUN QI

Nanjing University of Information Science and Technology, Nanjing, China, and Cooperative Institute for Mesoscale Meteorological Studies, University of Oklahoma, Norman, Oklahoma

(Manuscript received 21 September 2012, in final form 24 January 2013)

ABSTRACT

Previous analysis of Oklahoma City (OKC), Oklahoma, temperature data indicated that urban heat islands (UHIs) frequently formed at night and the observed UHI intensity was variable (1° – 4° C). The current study focuses on identifying meteorological phenomena that contributed to the variability of nocturnal UHI intensity in OKC during July 2003. Two episodes, one with a strong UHI signature and one with a weak signature, were studied in detail using observations along with simulations with the Weather Research and Forecasting model. Mechanical mixing associated with low-level jets (LLJs) played a critical role in moderating the nocturnal UHI intensity. During nights with weak LLJs or in the absence of LLJs, vertical mixing weakened at night and strong temperature inversions developed in the rural surface layer as a result of radiative cooling. The shallow stable boundary layer (SBL < 200 m) observed under such conditions was strongly altered inside the city because rougher and warmer surface characteristics caused vertical mixing that eroded the near-surface inversion. Accordingly, temperatures measured within the urban canopy layer at night were consistently higher than at nearby rural sites of comparable height (by $\sim 3^{\circ}$ – 4° C). During nights with strong LLJs, however, the jets facilitated enhanced turbulent mixing in the nocturnal boundary layer. As a consequence, atmospheric stability was much weaker and urban effects played a much less prominent role in altering the SBL structure; therefore, UHI intensities were smaller ($< 1^{\circ}$ C) during strong LLJs. The finding that rural inversion strength can serve as an indicator for UHI intensity highlights that the structure of the nocturnal boundary layer is important for UHI assessments.

Corresponding author address: Dr. Xiao-Ming Hu, Center for Analysis and Prediction of Storms, University of Oklahoma, Norman, OK 73072.
E-mail: xhu@ou.edu

1. Introduction

The ongoing, global trend of urbanization causes land-use changes at local and regional scales. Urban surfaces are rougher and typically also much drier than

rural surfaces, and the three-dimensional nature of urban landscapes further alters the radiation and surface energy balance. As a result, cities are known to affect weather and climate at multiple scales. One of the most widely known and intensively studied phenomena of urban weather modifications is the so-called urban heat island (UHI) effect, in which near-surface temperatures in metropolitan areas are typically higher than in the surrounding rural areas (Oke 1976, 1982; Arnfield 2003). Biophysical hazards such as heat stress, air pollution, and associated public health problems have been linked to UHI development (Zhang et al. 2009; Zhou and Shepherd 2010; Steeneveld et al. 2011; Chow et al. 2012; Fischer et al. 2012), which puts urban populations at even higher risks if the frequency of regional heat waves increases as a result of global climate change. Daily averages of UHI intensity, quantified as the difference between temperatures in the urban canopy layer and surrounding rural areas, have been reported to be 1°–3°C or even higher (Shahgedanova et al. 1997; Morris et al. 2001; Gedzelman et al. 2003; Liu et al. 2006; Grimmond 2007; Zhang et al. 2007; Fung et al. 2009; Miao et al. 2009; Mohan et al. 2012; Loughner et al. 2012; Brandsma and Wolters 2012).

The UHI intensity is related to the intrinsic characteristics of a city (Oke 1981, 1982; Grimmond 2007; Rizwan et al. 2008; Hidalgo et al. 2008; Nichol et al. 2009; Georgakis et al. 2010; Ryu and Baik 2012; Mohan et al. 2013) and external meteorological factors (Oke 1982; Mihalakakou et al. 2002). Oke et al. (1991) used a simple energy balance model to assess the relative importance of the commonly stated intrinsic causes of UHI under calm, cloudless conditions, including anthropogenic heat, thermal properties/moisture availability of the materials of the city, street canyon geometry, and urban greenhouse gases. The first three of these were identified as the main intrinsic causative factors contributing to the UHI intensity in a modeling study conducted by Ryu and Baik (2012). Mohan et al. (2013) also reported that the UHI intensity varies significantly in different parts of Delhi because of different densities of the built-up structures. The external meteorological factors known to modulate the UHI intensity include cloudiness, solar radiation, and wind speed (Unger et al. 2001; Morris et al. 2001; Fast et al. 2005; Souch and Grimmond 2006; Alonso et al. 2007; Steeneveld et al. 2011). The dependence of UHI intensity on the meteorological factors varies significantly among different times and different locations. Runnalls and Oke (1998) reported that nocturnal UHI magnitude decreased with increasing wind and cloudiness in Vancouver, British Columbia, Canada. Morris et al. (2001) found that the UHI in Melbourne, Australia, was inversely proportional to approximately

the fourth root of both the wind speed and the cloud amount but that the fidelity of the regression relationships varied among seasons because other factors may also become important. Fast et al. (2005) reported that summertime UHI in Phoenix, Arizona, decreased with increasing cloud cover whereas it showed negligible dependence on surface wind speed. In a study of the seasonal variation of UHI intensity of a Hungarian city, climatological cloudiness and wind speed were shown to play negative roles on the development of UHI in certain months of a year (Unger et al. 2001). An investigation of UHI intensity in Dutch cities generally showed a weak correlation with incoming solar radiation and surface wind speed, but the dependence varied among the different cities (Steenefeld et al. 2011). Even though the understanding of relevant factors, strength, and spatial extent of UHI phenomena advanced during the past few decades, methods to estimate and predict UHI intensity as a function of time, weather conditions, and structural attributes are still needed (Arnfield 2003). Stewart (2011) also stressed the need for better documentation of metadata for observation sites that are used to determine the UHI intensity and proposed the use of a local climate zone classification system instead of the typically used two-type classification into rural and urban sites (Stewart and Oke 2012).

In 2003, Oklahoma City, Oklahoma (OKC; 35.468 762°N, 97.516 304°W), spanned ~1610 km² and had a population of ~523 000. It is one of the 10 largest cities by land area in the United States. The urbanized area of OKC spanned ~630 km², which is significantly less than the total area. Embedded within the urbanized area is a well-defined central business district (CBD) that spanned ~20 km², with the average building height in 2003 being around 50–70 m and the tallest building being 152 m high (Burian et al. 2005). General characteristics of the UHI in OKC were investigated by Basara et al. (2008). During nighttime (roughly 2100–0600 local time), the UHI intensity in OKC was on average approximately 1.5°C in July of 2003, and the daytime UHI intensity decreased to approximately 0.5°C. Even though the nocturnal UHI was consistently observed, the intensity was variable, with values ranging between 1° and 4°C on individual nights (Basara et al. 2008; Klein et al. 2010). The observed diurnal variation of UHI intensity is consistent with the generally accepted view that the UHI is primarily a nocturnal phenomenon (Tumanov et al. 1999; Lemonsu and Masson 2002; Arnfield 2003; Souch and Grimmond 2006; Basara et al. 2008; Cui and de Foy 2012; Camilloni and Barrucand 2012). Open questions still remain about the factors that contribute to the day-to-day variability of the nocturnal UHI in OKC and in other cities.

Most of the UHI studies concluded that UHI signatures are strongest at night. Interactions between the UHI phenomena and other features of the nocturnal boundary layer (NBL) are thus of particular interest. The nocturnal low-level jet (LLJ), a stream of fast-moving air with a wind speed maximum in the lowest 2 km (Blackadar 1957; Hoecker 1963; Bonner 1968; Stull 1988; Whiteman et al. 1997), is one prominent feature of the NBL in the Great Plains of North America. The vertical shear of the horizontal wind associated with the nocturnal LLJ plays an important role in the generation of turbulence in the layer between the jet maximum or “nose” and the earth’s surface (Banta et al. 2003, 2006; Balsley et al. 2008). In contrast to the “traditional” boundary layer where turbulence is generated at the surface and transported upward, wind shear associated with LLJs can generate turbulence aloft and turbulence is transported downward, leading to the formation of the “upside down” boundary layer (Mahrt and Vickers 2002; Banta et al. 2006). Nocturnal LLJs form following the attenuation of daytime convective turbulent mixing, allowing nighttime winds above a stable boundary layer to accelerate to supergeostrophic wind speeds (Blackadar 1957; Parish and Oolman 2010). Other mechanisms can also contribute to the jet acceleration. Because of conservation of potential vorticity, northward-moving airflow can be accelerated as the Coriolis parameter increases with increasing latitude (Wexler 1961; Zhong et al. 1996). The diurnal heating and cooling cycle of terrain slopes can also contribute to the ageostrophic wind component at night through formation of the thermal wind, thus accelerating the LLJ (Holton 1967; Ryan 2004). On the basis of LLJ strength (i.e., wind maximum at the jet nose) and decrease in speed above the jet, LLJs are sometimes subjectively classified into three categories with LLJ strengths between 12 and 16 m s⁻¹, between 16 and 20 m s⁻¹, and above 20 m s⁻¹, respectively (Bonner 1968; Whiteman et al. 1997). The summertime Great Plains LLJ of the central United States has been the subject of numerous investigations during the past several decades (Wexler 1961; Zhong et al. 1996; Whiteman et al. 1997; Higgins et al. 1997; Parish and Oolman 2010). It is usually centered geographically over the southern Great Plains from Texas northward to Nebraska, with a maximum over northern Oklahoma and southern Kansas, and plays an important role in the transport of moisture, momentum, and air pollutants.

More recent studies focused on the climatological description of LLJs (Song et al. 2005, Zhang et al. 2006; Lundquist and Mirocha 2008), the role of topography in LLJ evolution (Ting and Wang 2006; He and Zhang 2010; Sun and Zhang 2012), improved analytical descriptions of the LLJ (Shapiro and Fedorovich 2009,

2010), and the influence of the LLJ on the structure, dynamics, and mixing in the NBL (Banta et al. 2002, 2003). To date, few measurements of LLJs in and near urban areas (e.g., De Wekker et al. 2004; Wang et al. 2007; Lundquist and Mirocha 2008; Kallistratova and Kouznetsov 2012) have been available. Wang et al. (2007) measured LLJ profiles with a Doppler lidar and two radar wind profilers during the Joint Urban 2003 (JU2003) tracer experiment (Allwine et al. 2004). Using range–height indicator scans from the lidar, they could study the impact of urban effects on LLJ height and strength. Over the urban area, the LLJs were ~25–100 m deeper and the velocities below the jet nose were ~10%–15% slower than over suburban terrain. De Wekker et al. (2004) and Lundquist and Mirocha (2008) also concluded that LLJs were frequently observed during the JU2003 experiment. Strong shear on the underside of the LLJ was found to induce strong turbulent mixing that can propagate downward to the surface (Banta et al. 2006; Lundquist and Mirocha 2008). Kallistratova and Kouznetsov (2012) conducted a study using sodars to measure LLJs in and near Moscow, Russia. They also observed higher and weaker jets in urban areas than at a rural site, which they explained by impacts of the UHI.

While these urban studies highlight that urban effects influence the LLJ dynamics, it remains unclear to what extent LLJ dynamics affect the UHI development and intensity. Since UHIs and LLJs are both frequently observed in the OKC metropolitan area, it is an ideal location to further study the interactions between these two nocturnal phenomena. In this study, the daily variation of nocturnal UHI intensity in OKC during July of 2003 and its relationship with LLJ development are thus investigated to test the hypothesis that shear-generated turbulent mixing below the LLJ nose plays an important role in modulating UHI intensity. To test this hypothesis, JU2003 observations of near-surface meteorological variables and boundary layer profiles were analyzed. Numerical simulations with the Weather Research and Forecasting (WRF) model, version 3.4 (Skamarock et al. 2008) were evaluated against data from the Oklahoma Mesonet (McPherson et al. 2007) and provided additional insight about regional-scale weather patterns and urban–rural contrasts. The simulations also enable assessment of the utility of rural inversion strength in predicting the strength of the UHI.

The paper is organized as follows. In section 2, the datasets and configurations of the WRF simulations used in this study are described. In section 3, the relationship between LLJs and UHI is statistically examined using observations and model simulations. The paper concludes in section 4 with a summary of the main findings and a discussion about the uncertainties of

model simulations and implications for future studies of LLJs.

2. Methods

a. Observations

The JU2003 tracer experiment (Allwine et al. 2004), a field experiment that was conducted in the OKC metropolitan area from 28 June to 31 July 2003 as a joint effort involving several government laboratories, universities, and private companies, primarily focused on providing datasets for the improvement and evaluation of urban dispersion models. In addition to tracer gas detectors, multiple meteorological observation systems were deployed across the OKC metropolitan area, including the systems discussed here that are most relevant to this study.

Boundary layer radar wind profilers were operated almost continuously during the entire month of July of 2003 in OKC by the Pacific Northwest National Laboratory (PNNL) and the Argonne National Laboratory (ANL; De Wekker et al. 2004). The PNNL and ANL sites were located approximately 2 km south and 5 km north of downtown OKC, respectively (Fig. 1b). The radar wind profilers collected data with a vertical resolution of 55 m and a consensus interval of 25 min. Lundquist and Mirocha (2008) investigated the LLJ properties during JU2003 using data from the profiler at the PNNL site. From their analysis, only four nights (i.e., 1, 11, 12, and 23 July) during the entire project did not meet the criteria for development of a LLJ at the PNNL site. Data below 300 m are not available from the PNNL wind profiler (Lundquist and Mirocha 2008), however, which limits the detectability of LLJs with a nose below 300 m (e.g., those on 1 and 11 July). In this study, we therefore used data from the ANL wind profiler, which provides coverage from 82 to ~2700 m (De Wekker et al. 2004), to investigate any possible links between LLJ dynamics and UHI trends.

Radiosonde profiles were measured at the PNNL site during four nighttime intensive observational periods (IOPs). Temperature profiles during two nighttime IOPs (i.e., 18–19 and 24–25 July) are included in the current analysis to illustrate the atmospheric stabilities during those nights.

Heat and momentum fluxes measured with sonic anemometers at two levels (37.3 and 79.6 m) installed at the Tyler Media (TM) tower were used to illustrate the impact of LLJs on turbulent mixing. The TM tower was operated by the University of Indiana and was located 5.5 km south of downtown OKC (Grimmond et al. 2004).

During JU2003, two datasets of near-surface temperature were collected in and near the OKC CBD by

two types of instruments deployed at two levels: 33 Onset Computer Corporation “HOBO” temperature dataloggers (Whiteman et al. 2000) deployed at 2 m above ground level (AGL), and 13 Portable Weather and Information Display Systems (PWIDS) stations deployed at 9 m AGL on traffic poles. The UHI intensity was determined at 2 and 9 m following the approach used in Basara et al. (2008), which was defined as

$$\Delta T = T_{\text{urban}} - T_{\text{rural}}. \quad (1)$$

The mean urban temperature T_{urban} for OKC at 2 and 9 m was calculated using temperature data collected by the HOBO and PWIDS instruments, respectively. The mean rural temperature T_{rural} at 2 and 9 m was calculated using the temperature observed at six Oklahoma Mesonet sites surrounding the OKC metropolitan area [El Reno (ELRE), Guthrie (GUTH), Kingfisher (KING), Minco (MINC), Norman (NRMN), and Spencer (SPEN); see Figs. 1b,c]. The Oklahoma Mesonet is a rural network with minimal influences from urban landscapes (McPherson et al. 2007; Basara et al. 2008). As a result of the urbanization in recent years, NRMN station was at the edge of an urban area by 2006 according to the U.S. Geological Survey (USGS) 2006 National Land Cover Data (NLCD; Fig. 1c), and rural sites to the north-northeast (SPEN especially) may be influenced by advection of warmer air from OKC, which could potentially result in an underestimation of the UHI intensity. The ELRE site west of the metropolitan area is known to experience rapid in situ cooling, however, that results in stronger and more frequent near-surface inversions than at other nearby mesonet sites (Hunt et al. 2007), which argues for using average values for assessing the rural background temperature. A more detailed description about the characteristics of both urban and rural stations was given by Basara et al. (2008). When comparing UHI intensities at 2 and 9 m, Basara et al. (2008) found that the average nighttime UHI was around 2°C at 2 m but decreased to 1.5°C at 9 m during JU2003. General characteristics of the UHI in OKC in July of 2003 were reported in Basara et al. (2008); the study presented here focuses on addressing the unresolved question regarding the day-to-day variation of the nocturnal UHI intensity in OKC. Since the 2-m urban observations were only recorded during the JU2003 experiment, we have decided to primarily use the 9-m UHI signal for our analysis. This will allow us to expand the study over a longer time period in the future. For selected episodes, however, a comparison of 2- and 9-m UHI intensities is presented in section 3.

Meteorological data collected by the Oklahoma Mesonet (McPherson et al. 2007) were also used in this study

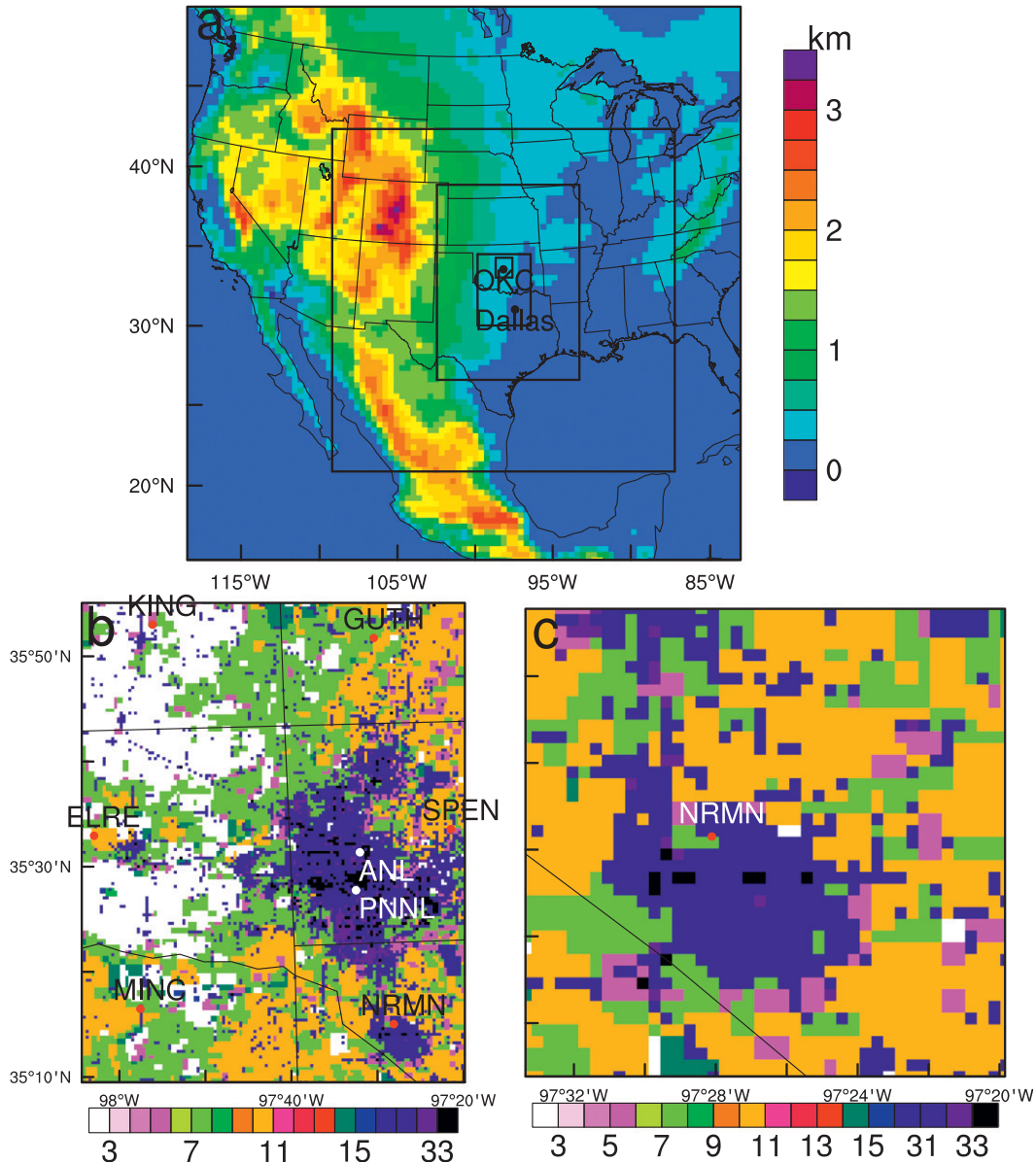


FIG. 1. (a) Map of model domains and terrain height, (b) land-use categories in the center part of domain 5, and (c) the same around NRMN as used in this study. The urban land-use categories (i.e., 31–33) were retrieved from the 2006 NLCD. The locations of six mesonet sites around OKC (i.e., ELRE, GUTH, KING, MINC, NRMN, and SPEN) and the ANL and PNNL sites are marked in (b). Land-use categories are defined below in Table 2.

for evaluating the WRF model output. The spacing between mesonet stations is approximately 30 km, and meteorological observations are collected and stored every 5 min (Fiebrich and Crawford 2001). The mesonet observations used in this study included air temperature at 1.5 and 9 m AGL and wind speed at 10 m AGL.

b. Three-dimensional simulations

To investigate the relationship between LLJs and UHI, three-dimensional WRF (Skamarock et al. 2008)

simulations were conducted for four nights (17/18, 18/19, 24/25, and 25/26 July), which were selected as study periods after analyzing the JU2003 data. Four 44-h simulations were initialized at 0000 UTC on 17, 18, 24, and 25, July, respectively. Five one-way nested domains (Fig. 1a) were employed, with horizontal grid spacings of 40.5, 13.5, 4.5, 1.5, and 0.5 km, respectively. Each domain had 48 vertical layers extending from the surface to 100 hPa. The model sigma levels and midlayer heights of the lowest 20 model layers are shown in Table 1. All

TABLE 1. Sigma levels and midlayer heights (m AGL) of the lowest 20 model layers. The sigma levels are defined as $(p - p_{\text{top}})/(p_{\text{surf}} - p_{\text{top}})$, where p is the dry hydrostatic pressure at each corresponding level, p_{surf} is the dry hydrostatic surface pressure, and p_{top} is a constant dry hydrostatic pressure at model top.

| Sigma level | Midlayer height | Sigma level | Midlayer height |
|-------------|-----------------|-------------|-----------------|
| 1.0 | 12 | 0.94 | 459 |
| 0.997 | 37 | 0.93 | 545 |
| 0.994 | 61 | 0.92 | 631 |
| 0.991 | 86 | 0.91 | 717 |
| 0.988 | 111 | 0.895 | 826 |
| 0.985 | 144 | 0.88 | 958 |
| 0.975 | 186 | 0.865 | 1092 |
| 0.97 | 227 | 0.85 | 1226 |
| 0.96 | 290 | 0.825 | 1409 |
| 0.95 | 374 | 0.8 | 1640 |

model domains used the Dudhia shortwave radiation algorithm (Dudhia 1989), the Rapid Radiative Transfer Model (Mlawer et al. 1997) for longwave radiation, and the WRF single-moment six-class (WSM6) microphysics scheme (Hong et al. 2004). The Yonsei University (YSU; Hong et al. 2006) planetary boundary layer (PBL) scheme was initially chosen, but it was noted that LLJ strength was underestimated by YSU. Previous studies concluded that nonlocal mixing schemes such as the YSU scheme tend to simulate weaker LLJs because of unrealistic, strong momentum mixing during nighttime (Storm et al. 2008; Hu et al. 2010; Shin and Hong 2011; Floors et al. 2013). The Asymmetric Convective Model, version 2 (ACM2), scheme (Pleim 2007a,b) considers nonlocal mixing during the daytime but uses a local mixing approach in the stable boundary layer. It performs well during the daytime when a nonlocal scheme is essential for capturing mixing by large-scale convective motions (Hu et al. 2010; Kolling et al. 2012; Draxl et al. 2013). At night, the local scheme limits the vertical mixing, which results in more realistic wind speed gradients (Shin and Hong 2011; Xie et al. 2012). Thus, the ACM2 scheme was selected for the simulations presented in this study. To simulate the thermodynamic and dynamic effects of urban areas on the atmosphere, the ‘‘Noah’’ land surface scheme (Chen and Dudhia 2001) coupled with a single-layer urban canopy model (UCM; Kusaka et al. 2001) was chosen. To assess the impact of urbanization on living environments and risks, this approach was applied to a few regions, including Houston, Texas (Jiang et al. 2008; Chen et al. 2011a); Washington, D.C., and Baltimore, Maryland (Zhang et al. 2009); the Pearl River Delta and Yangtze River Delta regions of China (Wang et al. 2009); Taipei, Taiwan (Lin et al. 2008); and Beijing, China (Miao and Chen 2008; Miao et al. 2009, 2011).

TABLE 2. Land-use categories used in the WRF simulations.

| Land-use category | Land-use description |
|-------------------|--|
| 1 | Urban and built-up land |
| 2 | Dryland cropland and pasture |
| 3 | Irrigated cropland and pasture |
| 4 | Mixed dryland/irrigated cropland and pasture |
| 5 | Cropland/grassland mosaic |
| 6 | Cropland/woodland mosaic |
| 7 | Grassland |
| 8 | Shrubland |
| 9 | Mixed shrubland/grassland |
| 10 | Savanna |
| 11 | Deciduous broadleaf forest |
| 12 | Deciduous needleleaf forest |
| 13 | Evergreen broadleaf |
| 14 | Evergreen needleleaf |
| 15 | Mixed forest |
| 16 | Water bodies |
| 31 | Low-intensity residential |
| 32 | High-intensity residential |
| 33 | Industrial/commercial |

The urban land-use categories (Figs. 1b,c; Table 2) were derived from the NLCD 2006, in which the urban land use was divided into three categories: low-intensity residential (31), high-intensity residential (32), and commercial/industrial (33). For regions other than the urban area, the USGS land-use and soil-category data with resolutions of 10', 5', 2', 30'', and 30'' were used in each domain. The North American Regional Reanalysis with a resolution of approximately $0.3^\circ \times 0.3^\circ$ (32 km) was used for the initial and boundary conditions of all meteorological variables.

3. Results

Satellite-derived land surface temperature is commonly used as a surrogate for the air temperature to analyze the UHI spatial distribution (Voogt and Oke 2003; Brown et al. 2004; Goldreich 2006; Fung et al. 2009; Zhou and Shepherd 2010). Monthly mean daytime and nighttime land surface temperatures in July 2003, retrieved from Moderate Resolution Imaging Spectroradiometer (MODIS) data, clearly depict the nocturnal UHI (Fig. 2). During nighttime, urban effects were prominent around large metropolitan areas, including OKC and Dallas–Fort Worth, Texas (DFW), whereas such an effect cannot be clearly identified in the daytime spatial distribution, confirming the findings of Basara et al. (2008) that the UHI is primarily a nocturnal phenomenon in OKC. From Fig. 2a, it can also be noticed that the urban area of OKC is smaller than that of DFW and nighttime temperatures are lower in OKC

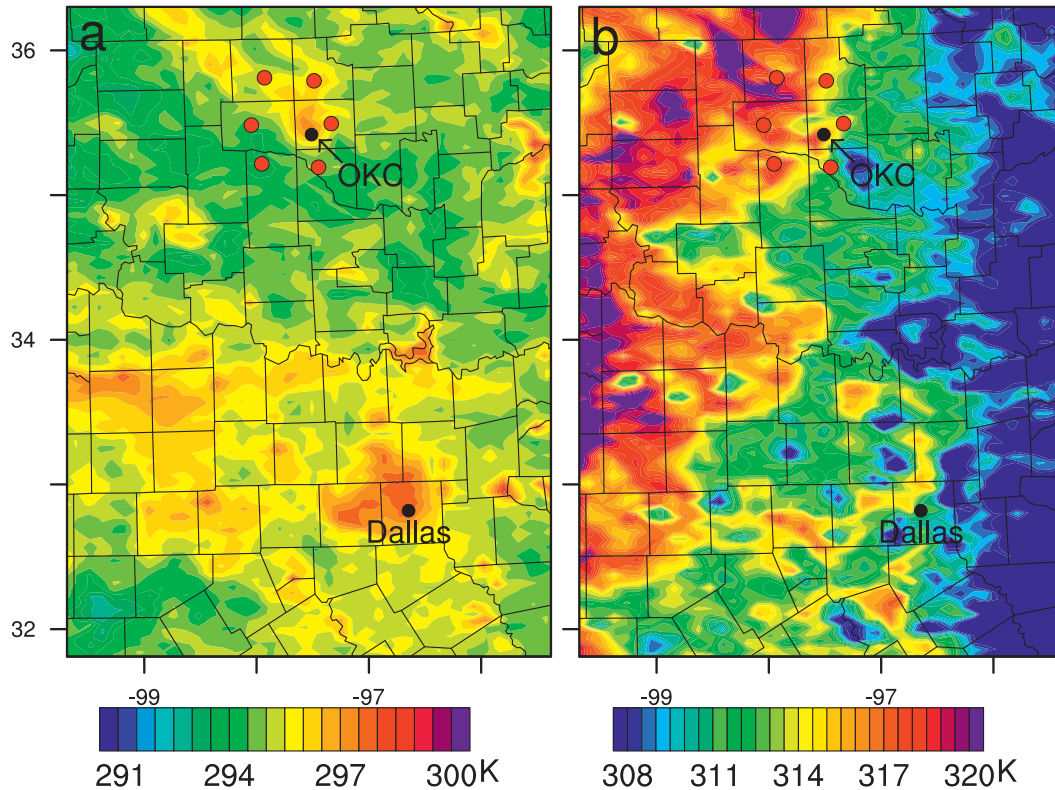


FIG. 2. MODIS-detected land surface temperature during (a) nighttime and (b) daytime in July 2003. Red dots highlight the six Oklahoma Mesonet sites around OKC.

than in DWF, confirming previous findings that nocturnal UHI intensity increases with city size (Arnfield 2003). While the UHI intensities reported in this study may thus underestimate the impact of larger cities on the thermal climate, the datasets available for OKC provided a unique opportunity to investigate the role of synoptic conditions in modulating UHI intensity.

As discussed in the introduction, the Great Plains LLJ is frequently observed in and near OKC, and shear-generated turbulence below the jet nose can strongly influence turbulent mixing and the structure of the NBL (Banta et al. 2003, 2006; Lundquist and Mirocha 2008). The LLJ will thus likely also affect the nocturnal UHI intensity. Nocturnal turbulence kinetic energy (TKE) was reported to scale better with LLJ strength (i.e., the maximum wind speed at the jet nose) than with some surface variables. Thus, LLJ strength is likely a key factor in modulating the structure of the NBL and UHI intensity (Banta et al. 2003, 2006). The relationship between LLJ strength and mean nocturnal UHI intensity in July of 2003 is illustrated in Fig. 3. Lundquist and Mirocha (2008) used a maximum wind speed larger than 10 m s^{-1} followed by a decrease above this maximum of at least 5 m s^{-1} as LLJ criteria. On 1, 11, 12, 23, and 31 July, such

LLJ criteria were not met as shown by the PNNL wind profiler data, but upon further analysis of the ANL wind profiler data a local wind speed maximum existed in the boundary layer. Thus, the local maximum wind speeds in the lower 800 m AGL at night were taken as the LLJ strength in our study. The mean nocturnal UHI intensity for each night was computed using the temperature differences ΔT in (1) for the time window [2115–0620 central standard time (CST); CST = UTC – 6 h] during which the OKC UHI was most prominent in July of 2003 (Basara et al. 2008). The mean nocturnal UHI intensity showed significant inverse correlation with the strength of the LLJs (with a Pearson's correlation coefficient of -0.81 ; Fig. 3). The observed vertical wind profiles at various locations in the OKC metropolitan area (including the CBD wake, CBD, urban, suburban, and rural) showed that LLJ strength varied very little ($<0.5 \text{ m s}^{-1}$) at those locations (Wang et al. 2007). Thus, the impact of urban effects on LLJ strength is negligible and it is unlikely that urban effects can change the daily nocturnal LLJ strength by more than 10 m s^{-1} as observed during JU2003. Therefore, the high correlation shown in Fig. 3 can only suggest that variations in LLJ strength played an important role in modulating the UHI intensity.

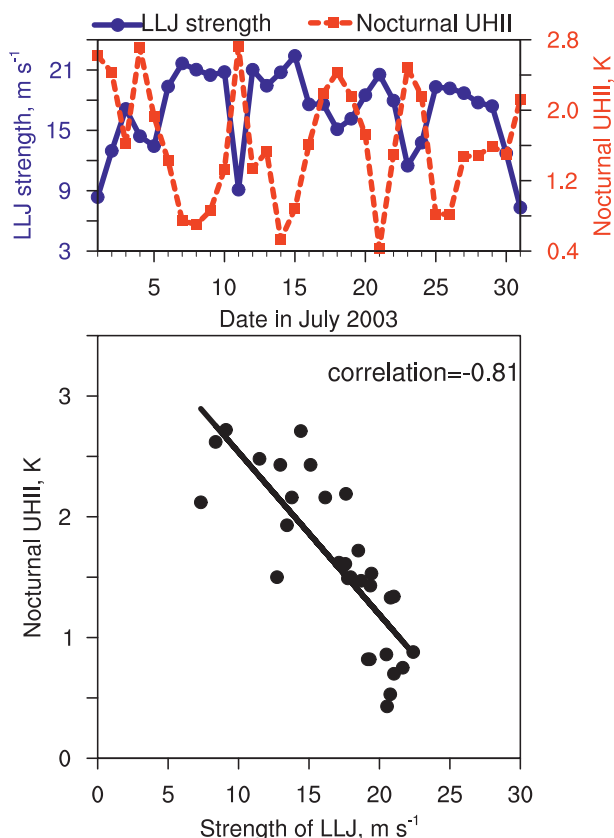


FIG. 3. (top) Time series of observed mean nocturnal UHI intensity (UHII) at 9 m and strength of LLJ (maximum wind speed at the jet nose) over OKC in July 2003 and (bottom) their correlation. As reported in Basara et al. (2008), the UHI in OKC during JU2003 was most prominent between 2115 and 0620 CST; therefore, the mean nocturnal UHII was computed over this time window.

To better understand the role of the LLJ in modulating the UHI, two nights with strong UHI intensities (i.e., the nights of 17/18 and 18/19 July) and two nights with weak UHI intensities (i.e., the nights of 24/25 and 25/26 July) were chosen for further investigation. As determined from MODIS satellite images, the sky was

clear on these four nights. Figure 4 shows the time series of UHI intensity at 2 and 9 m in OKC on those days. As expected from the analysis of Basara et al. (2008), the daytime UHI intensity in OKC was weak, negligible, or even negative, especially at 2 m. UHI intensity increased prominently around the evening transition and then stayed at a roughly constant level throughout the night. These UHI characteristics in OKC are consistent with findings for other cities, such as Bucharest, Romania (Tumanov et al. 1999); Paris, France (Lemonsu and Masson 2002); and London, United Kingdom (Bohnenstengel et al. 2011). Clear differences in UHI intensity emerge on different nights: during the nights of 17/18 and 18/19 July the mean UHI intensity was 2.4°C (9 m), whereas the mean UHI intensity was only 0.8°C (9 m) on the nights of 24/25 and 25/26 July. UHI intensity increased by $\sim 1^{\circ}\text{C}$ when computed at 2 m for the nights of 17–19 July, and it stayed the same for the nights of 24–26 July. Brown et al. (2004) also reported UHI intensities determined by mobile measurements from a car that drove across the OKC metropolitan area along different routes transecting rural, suburban, and urban terrain for the two chosen time periods. During 25/26 July, the UHI intensity ($\sim 0.9^{\circ}\text{C}$) tended to be lower than during the nights of 17–19 July ($\sim 4.5^{\circ}\text{C}$). Hereinafter, 17–19 July is referred to as the strong-UHI episode and 24–26 July is referred to as the weak-UHI episode. The analyses presented in the remainder of this paper focus on identifying the causes of the pronounced differences in UHI intensity during these two episodes.

The stability and nocturnal boundary layer structure for the strong-UHI episode and the weak-UHI episode showed distinct differences, which are illustrated in the potential temperature profiles measured by the radiosondes released at the PNNL site (Fig. 5). Strong temperature inversions developed near the surface on the night of 18/19 July (Fig. 5a), and a much weaker inversion (nearly neutral) yet thicker boundary layer developed on the night of 24/25 July (Fig. 5b) in the presence

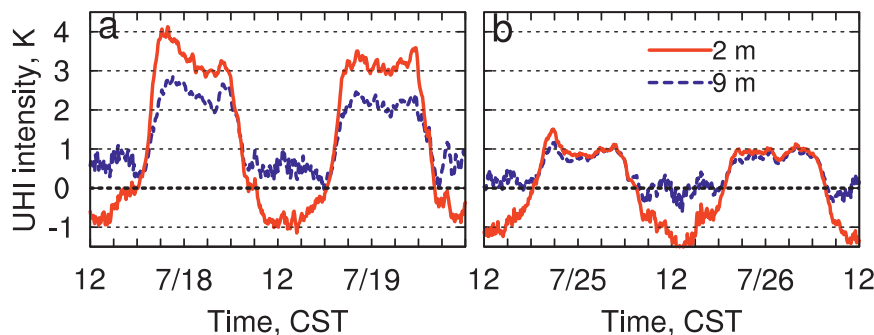


FIG. 4. Time series of observed UHI intensity at 2 and 9 m on days with (a) strong and (b) weak UHIs.

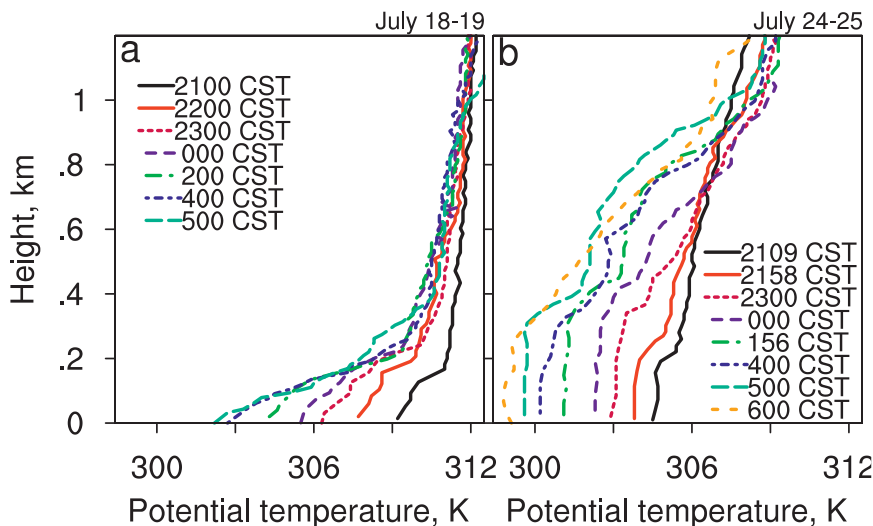


FIG. 5. Vertical profiles of observed potential temperature at the PNNL site (a) on the night of 18/19 July with strong UHI and (b) on the night of 24/25 July with weak UHI.

of a strong LLJ, with the maximum wind speed at the jet nose as strong as 19.3 m s^{-1} . The nearly neutral nocturnal boundary layer explains the similar UHI intensities evaluated at both 2 and 9 m on the nights of the weak-UHI episode (Fig. 4b). It is hypothesized that 1) stronger LLJs occur with weaker temperature inversions and vice versa and that 2) the environmental temperature inversion strength is a useful indicator for UHI intensity.

Synoptic-scale weather conditions have been reported to affect the UHI intensity by a few studies (Unger 1996; Tumanov et al. 1999; Morris and Simmonds 2000; Mihalakakou et al. 2002). Synoptic surface weather maps at 0600 CST are displayed in Fig. 6 to examine the similarities and differences among the large-scale forcings on the four nights. During the strong-UHI episode, the pressure gradient was relatively weak in Oklahoma, resulting in low to moderate wind speeds. On the nights of the weak-UHI episode, high pressure centers resided in the eastern United States and extended westward into the southern Great Plains. The pressure gradient over most of the Great Plains is from east to west or southeast to northwest. Such pressure gradients and the blocking effect of the Rockies forced airflow from southerly latitudes into the south-central United States, thus contributing to the acceleration of the southerly or southwesterly LLJs during nighttime (Wexler 1961; Zhong et al. 1996). As a result, stronger LLJs were detected over OKC during the weak-UHI episode. On those nights, the maximum wind speeds at jet-nose level were as high as $>19 \text{ m s}^{-1}$ (Figs. 7c,d), whereas the maximum wind speeds on the nights of the strong-UHI episode were 15 and 16 m s^{-1} (Figs. 7a,b). The LLJ strengths (i.e., the maximum wind speed) of the weak- and strong-UHI

episodes fall into LLJ categories 1 and 2, respectively (Bonner 1968; Whiteman et al. 1997).

Three-dimensional WRF simulations were conducted to investigate further the role of the LLJ characteristics on UHI development and intensity. The WRF simulations successfully capture the contrast of LLJ strength on the four nights. Stronger LLJs are simulated on the nights of the weak-UHI episode (Figs. 7g,h), and weaker LLJs are simulated on nights of the strong-UHI episode (Figs. 7e,f) even though a certain degree of model bias exists (Figs. 7i-l). The levels of the jet noses simulated by the WRF model are also consistent with the observations (Fig. 7).

The spatial distributions of 10-m wind speed at 1000 UTC (0400 CST) on the four nights are displayed in Fig. 8. The observations from the Oklahoma Mesonet (McPherson et al. 2007) are overlaid for evaluation. The WRF simulations capture the differences between the selected two episodes and the spatial distribution of wind speed on each day. During the strong-UHI nights, lower 10-m wind speeds persisted over most of Oklahoma (Figs. 10a,b), and wind speeds were higher during the nights of the weak-UHI episode (Figs. 10c,d). The simulations further reproduced the prominent spatial wind speed gradient in Oklahoma on the nights of the weak-UHI episode, with wind speeds increasing from southeast to northwest (Figs. 8c,d).

The WRF simulations also captured the temperature distributions near the surface during both episodes very well (Fig. 9). For the weak-UHI episode, the model predicts a pronounced east-to-west temperature gradient (Figs. 9c,d) that appears to be correlated with the wind speed gradient shown in Figs. 8c and 8d. Similar trends are also seen in the observations.

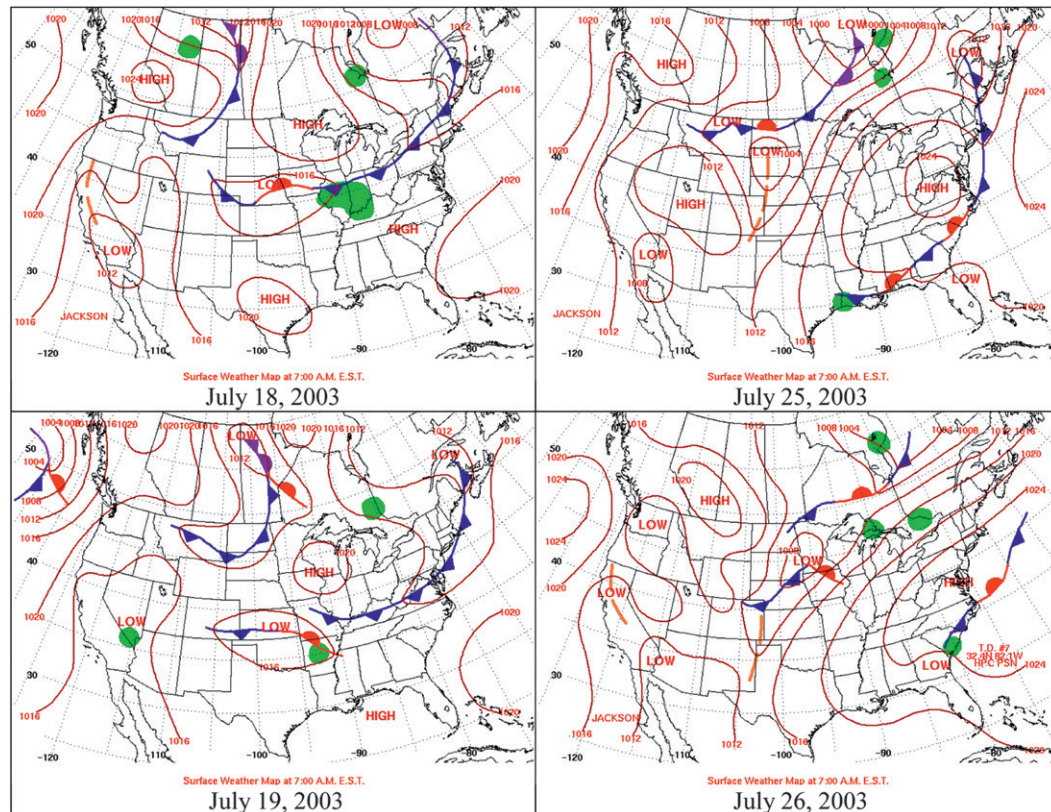


FIG. 6. Surface weather maps on days with (left) strong and (right) weak UHIs. The surface weather map was prepared and archived by the Hydrometeorological Prediction Center of the National Centers for Environmental Prediction (<http://www.hpc.ncep.noaa.gov/dailywxmap/>).

The spatial distribution of the winds at ~ 500 m above the surface (Fig. 10) shows weak LLJs on the nights of the strong-UHI episode and vice versa. The synoptic-scale pressure gradients (Fig. 6) and the terrain (Fig. 1a) play critical roles in determining the spatial distribution of the LLJs. On the nights of the weak-UHI episode, air in the Great Plains flowed northward without interception (Figs. 10c,d). The LLJs on those nights covered a wide region extending from Texas to Wisconsin and Michigan, which can be attributed to multiple factors, including a stronger pressure gradient (Fig. 6), southerly thermal wind induced by stronger nocturnal radiative cooling over the Rocky Mountains (Holton 1967), and an increase of the anticyclonic vorticity of northward-moving flow as a result of meridional variation of the Coriolis parameter (Wexler 1961; Zhong et al. 1996). Note that winds around OKC are westerly on the strong-UHI nights and are southerly on the weak-UHI nights. Because of the closeness and position of SPEN (the mesonet site at the east edge of OKC; Fig. 1b) to the urban area, its surface temperature was higher than at the other rural reference sites during the strong-UHI nights (not shown). Advection of hotter urban air by the

westerly wind could thus have caused an underestimation of the UHI intensity during this episode, but by choosing an average value that is based on six rural reference sites low or high biases of individual sites for different atmospheric conditions are minimized.

Strong shear associated with strong LLJs caused strong turbulent mixing in the nocturnal boundary layer (Fig. 11). Friction velocities and TKE were measured with sonic anemometers on a tall tower approximately 5 km south of downtown OKC (Grimmond et al. 2004). The measurements taken at an elevation of 37 m above ground were used to investigate turbulent mixing during the two episodes. During the strong-UHI episode, the friction velocities and TKE showed a distinct diurnal variation: when the relatively weak LLJ persisted at night (Figs. 11a,e), friction velocities dropped down to less than 0.2 m s^{-1} (less than 30% of the daytime values) and TKE decreased to negligible levels (Fig. 11c). Such strong diurnal variations were not observed during the weak-UHI episode: the friction velocities ($>0.4 \text{ m s}^{-1}$) and TKE ($\sim 1\text{--}2 \text{ m}^2 \text{ s}^{-2}$) remained elevated at night (Fig. 11d) as strong LLJs developed in the region (Figs. 11b,f). These elevated friction velocities and TKE indicate

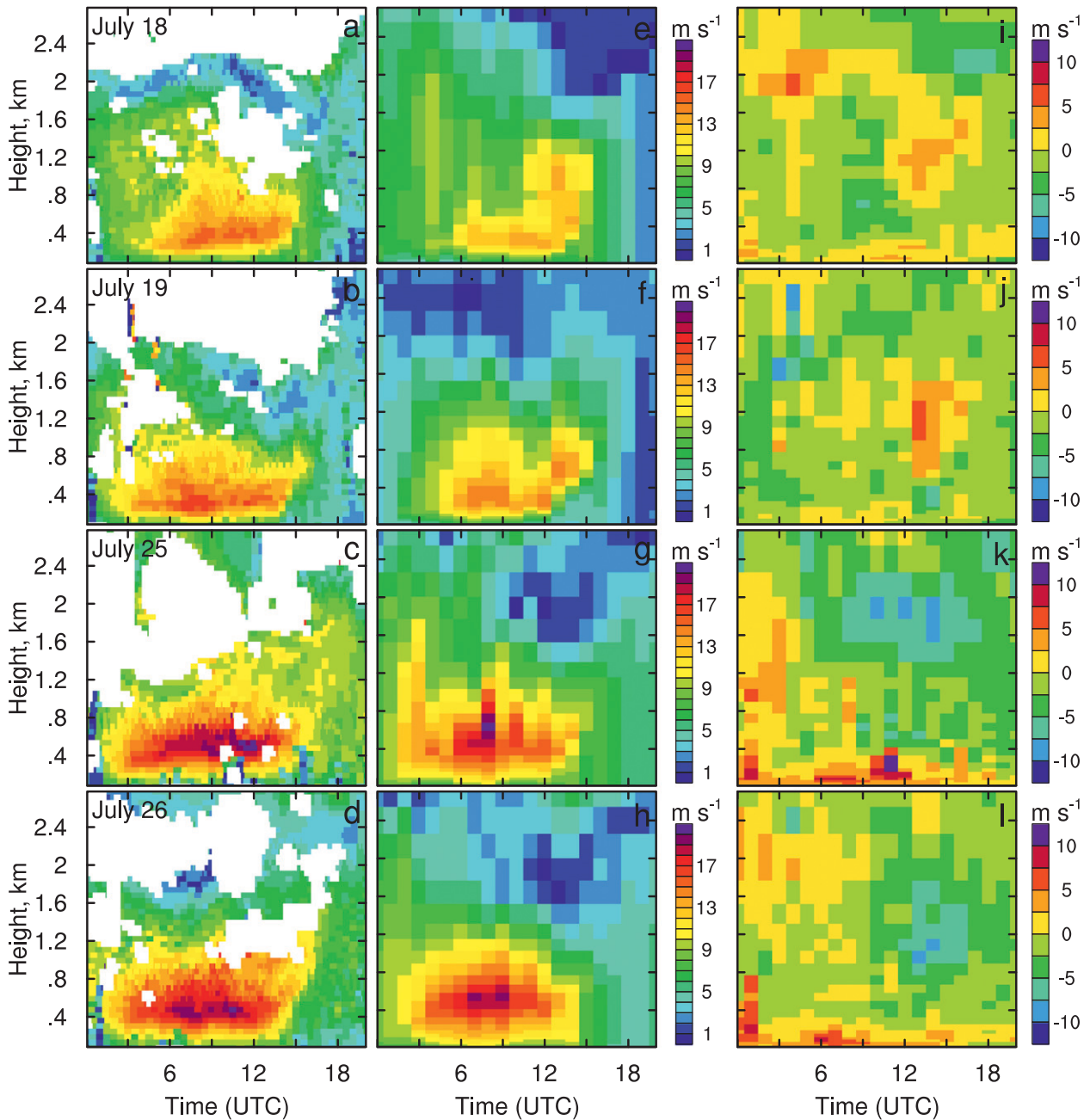


FIG. 7. Time–height diagrams of horizontal wind speed (a)–(d) observed by the boundary layer wind profiler and (e)–(h) simulated by the WRF model and (i)–(l) the model bias (simulated – observed) of horizontal wind speed at the ANL site on (top to bottom) 18 and 19 July (with strong UHI) and 25 and 26 July (with weak UHI). The observed values were interpolated to model levels and time during the calculation of model bias.

enhanced turbulent mixing in the nocturnal boundary layer in the presence of strong LLJs. Lundquist and Mirocha (2008) also reported persistent elevated turbulence in the nocturnal boundary layer on the night of 24/25 July induced by the strong LLJ.

Previous studies have shown that turbulent mixing in the nocturnal boundary layer plays an important role in

modulating the temperature-inversion strength near the ground. Light wind speeds and clear skies typically favor strong nocturnal radiative cooling in a thin boundary layer (Acevedo and Fitzjarrald 2001; Poulos et al. 2002). Fast et al. (2005) reported that mechanical mixing associated with larger wind speeds reduces or eliminates nocturnal radiational cooling by mixing warmer air from

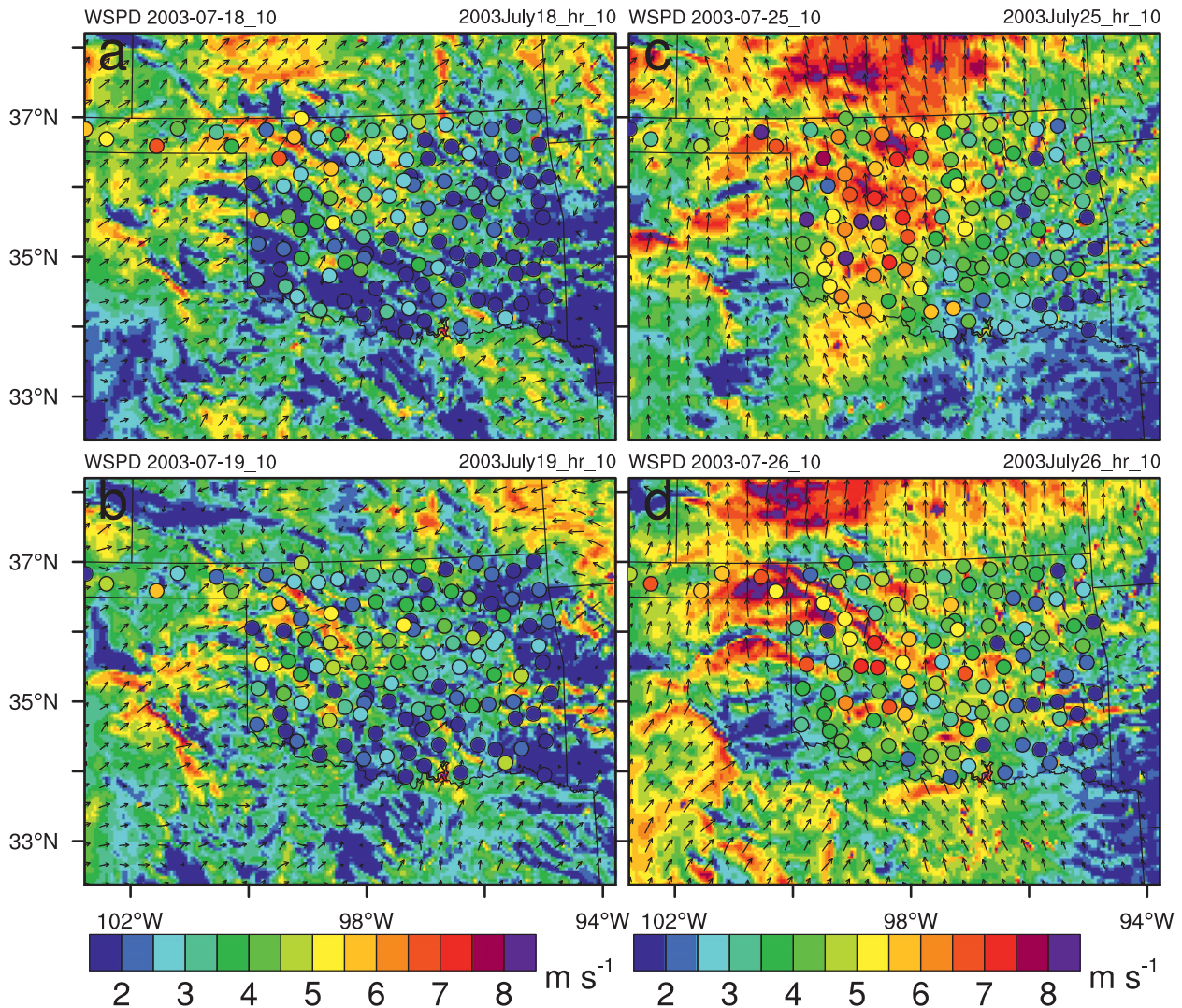


FIG. 8. Spatial distribution of simulated wind speed at 10 m AGL in domain 3 at 1000 UTC on days with (a),(b) strong and (c),(d) weak UHIs. The observed values at the Oklahoma Mesonet sites are indicated by shaded circles.

aloft down to the surface. The radiosonde profiles (Fig. 5 and corresponding discussion) provided evidence that the thermal structure within the NBL was different during the two episodes. Spatial distributions of the inversion strength (or vertical temperature gradient) across Oklahoma as observed at the Oklahoma Mesonet sites and as predicted by the WRF simulations (Fig. 12) allow further assessment of the role of the LLJ in triggering these differences. At 1000 UTC, the observed mean temperature inversion at all of the Oklahoma Mesonet sites near the surface was $0.16^{\circ}\text{C m}^{-1}$ on 18 July and $0.17^{\circ}\text{C m}^{-1}$ on 19 July, as compared with $0.04^{\circ}\text{C m}^{-1}$ on 25 July and $0.05^{\circ}\text{C m}^{-1}$ on 26 July. The corresponding values from the WRF simulations were 0.11, 0.15, 0.03, and $0.03^{\circ}\text{C m}^{-1}$, respectively. The reduced turbulent mixing

associated with a weaker LLJ promoted strong cooling near the surface, decoupling of the surface layer from the above residual layer, and thus strong temperature inversions during the two nights of the strong-UHI episode (Figs. 12a,b; also see temperature profiles in Fig. 5a for the strong temperature inversion on the night of 18/19 July). During the second episode (weak UHI), the stronger LLJ contributed to enhanced downward transport of warmer air from aloft that counterbalanced the radiational cooling near the surface and thus resulted in much weaker temperature inversions (Figs. 12c,d; also see Fig. 5b for the nearly neutral temperature profile near the surface on the night of 24/25 July). The role of the LLJ in moderating the temperature inversions during the weak-UHI episode is further supported by the

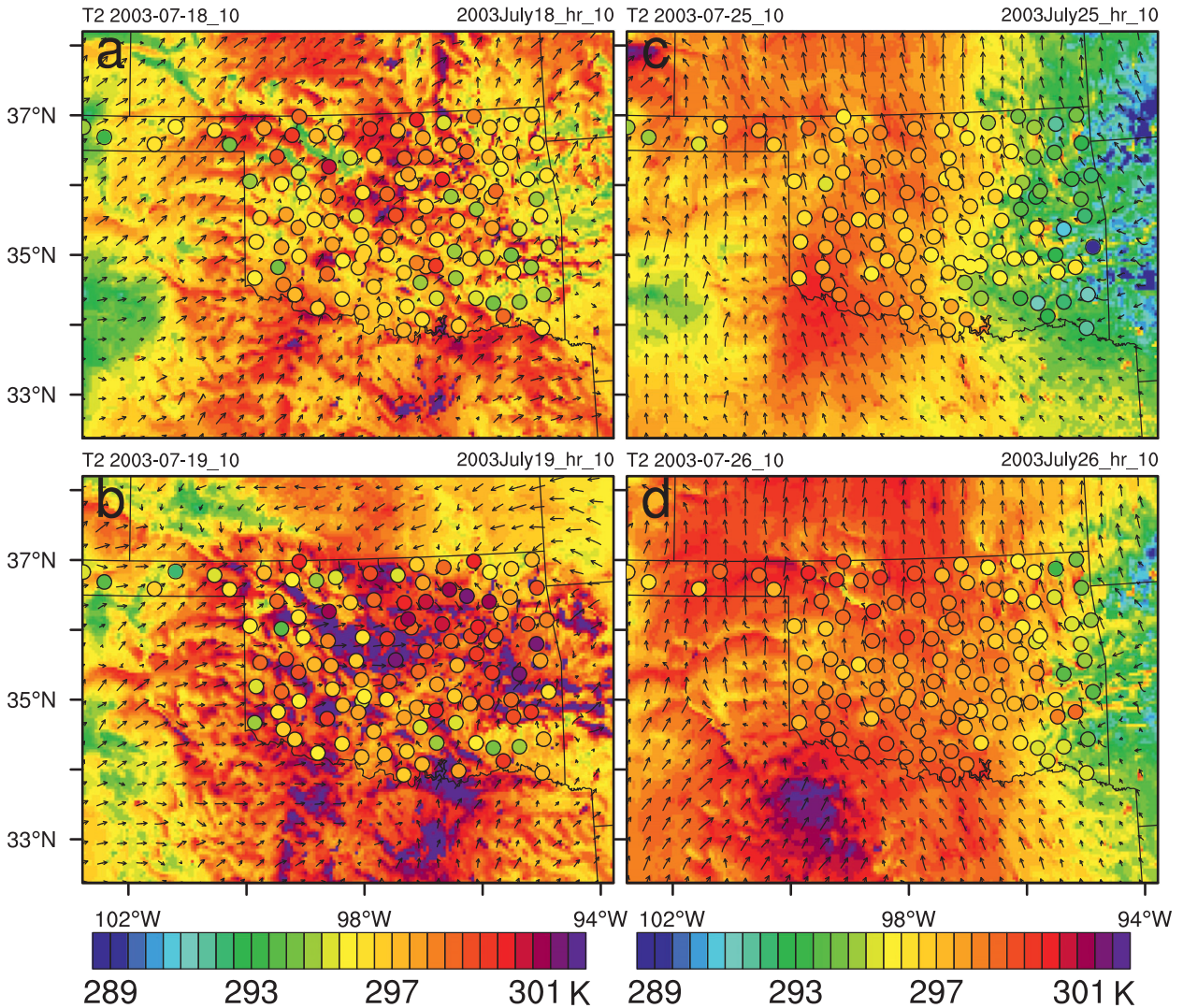


FIG. 9. Temperature at 2 m (T2) in domain 3 at 1000 UTC on days with (a),(b) strong and (c),(d) weak UHIs. Wind vectors show the simulated 10-m wind field. The observed values of temperature are indicated by shaded circles.

observed and simulated spatial correlations of wind speed and inversion-strength gradients during the weak-UHI episode: in eastern Oklahoma, where lower wind speeds persisted near the ground and aloft (Figs. 8c,d and 10c,d), the inversion strength is higher (Figs. 12c,d).

The WRF model output further allows investigation of the rural–urban contrasts in the thermal structure of the NBL during the two episodes. For this purpose, average vertical temperature profiles that are based on the WRF model output for the urban PWIDS and rural mesonet sites are compared in Fig. 13. The model simulations captured the distinct boundary layer characteristics on the night of 18/19 and 24/25 July, as shown in Fig. 5. In rural terrain, strong inversions developed on the nights of the strong-UHI episode in the lower

~200 m AGL (Figs. 13a,b). It appears that during this episode limited vertical mixing leads to strong radiational cooling within a shallow stable layer (~200 m) in rural terrain. At the urban sites, where urban land cover releases heat and vertical mixing is stronger because of the enhanced roughness, vertical temperature gradients are reduced and cooling near the surface is much weaker than in rural areas (Figs. 13a,b). As a consequence, a large difference between urban and rural near-surface temperatures—that is, a large UHI intensity (3°–4°C)—is observed on these nights. During the weak-UHI episode, vertical mixing associated with stronger LLJs limited the cooling at the rural sites and the NBL became much deeper (~500 m). Under these conditions, differences between the rural and urban profiles are

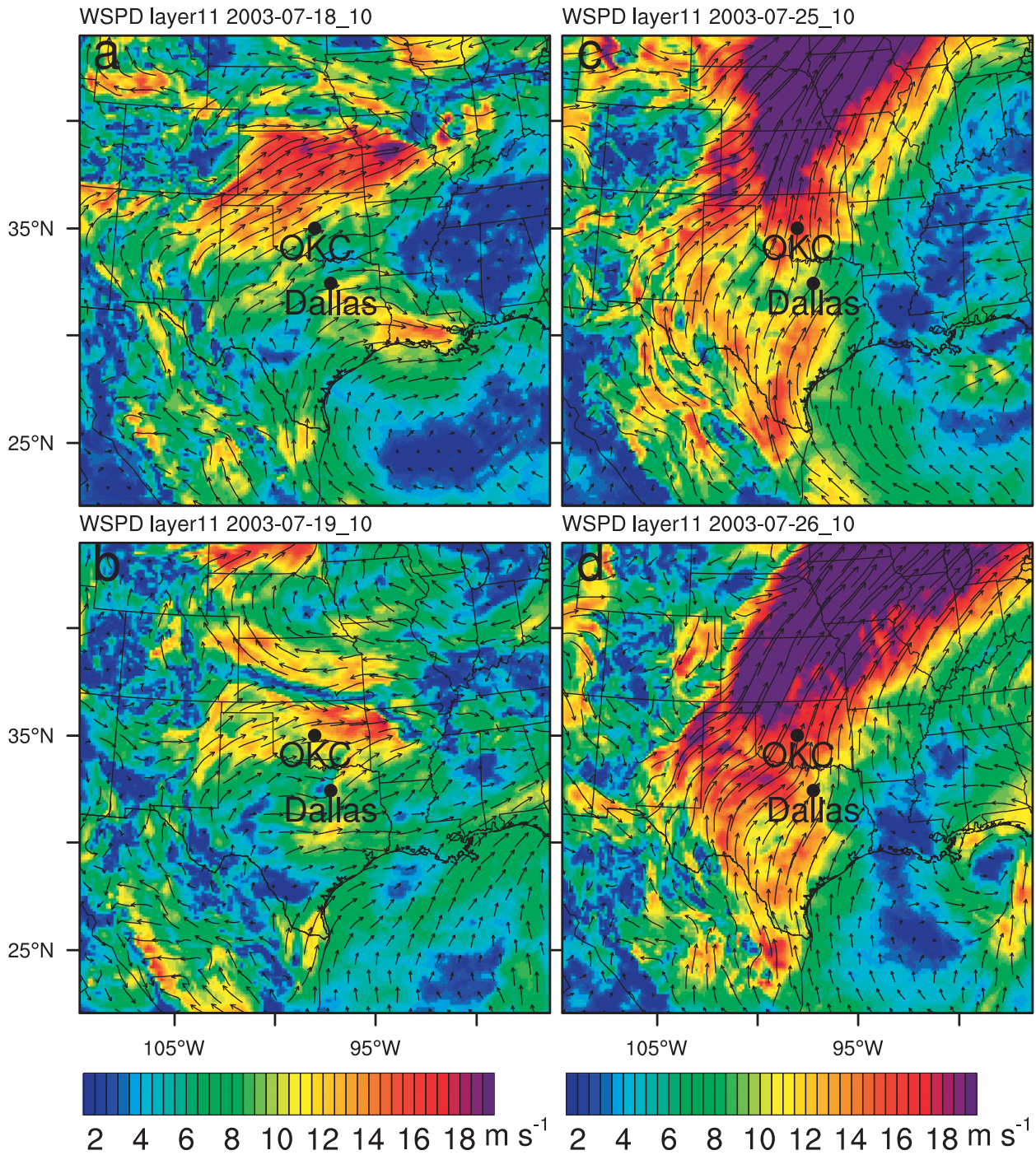


FIG. 10. Simulated wind speed at ~ 500 m AGL in domain 2 at 1000 UTC on days with (a),(b) strong and (c),(d) weak UHIs.

small and are limited to the lowest grid cells. In the presence of stronger LLJs, heat released from urban land cover is mixed over a deeper boundary layer and advected further downwind, which also contributed to the smaller temperature difference between the rural and urban areas. During both episodes, UHI intensity

declined with height and at some distance above the surface (~ 150 m) the urban temperature became lower than that in the surrounding rural area (i.e., the UHI signal reversed). This behavior is consistent with the classical conceptual model of UHI (Bornstein 1968; Oke 1982).

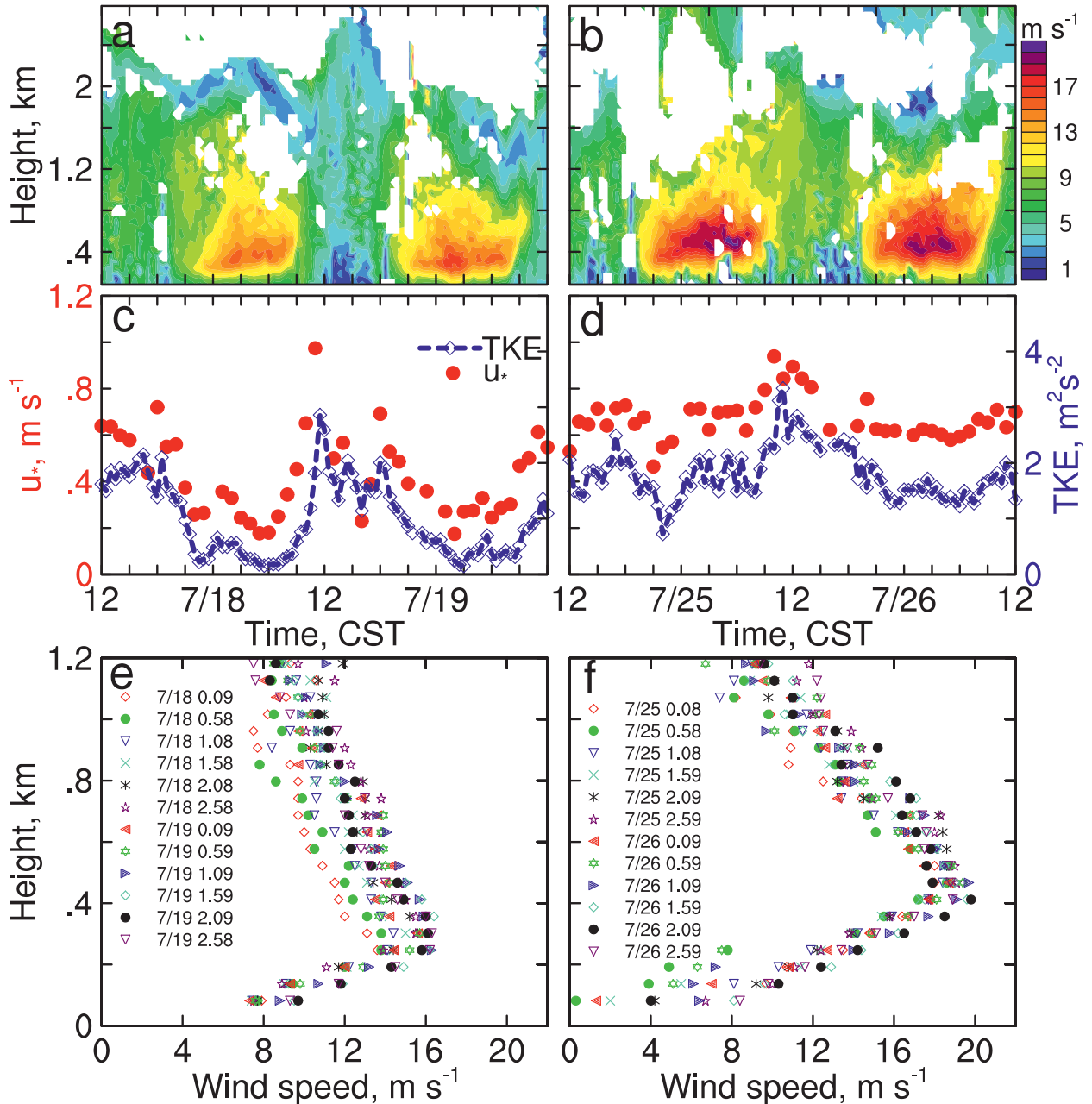


FIG. 11. (a),(b) Time–height diagram of horizontal wind speed observed by the boundary layer wind profiler, (c),(d) time series of observed frictional velocity u_* and TKE at ~ 37 m above ground, and (e),(f) vertical profiles of horizontal wind speed on (left) days with strong UHI and (right) days with weak UHI.

The corresponding wind profiles (Fig. 14) simulated with the WRF model for the same sites as the temperature profiles provide further evidence that the low-level jet was much stronger and higher during the weak-UHI episode than during the strong-UHI episode. Differences can also be noted in the height of the jet nose, which was at ~ 250 m for the strong-UHI episode and ~ 500 m for the weak-UHI episode. During both episodes,

the jet-nose height correlated well with the depth of the inversion layer. In comparison with the temperature profiles, the urban effects on the wind profiles are much weaker, and, while previously observed tendencies for higher and weaker urban LLJs (Wang et al. 2007; Kallistratova and Kouznetsov 2012) can be noted, they are not consistent among the four nights investigated. Future studies with more detailed observations and

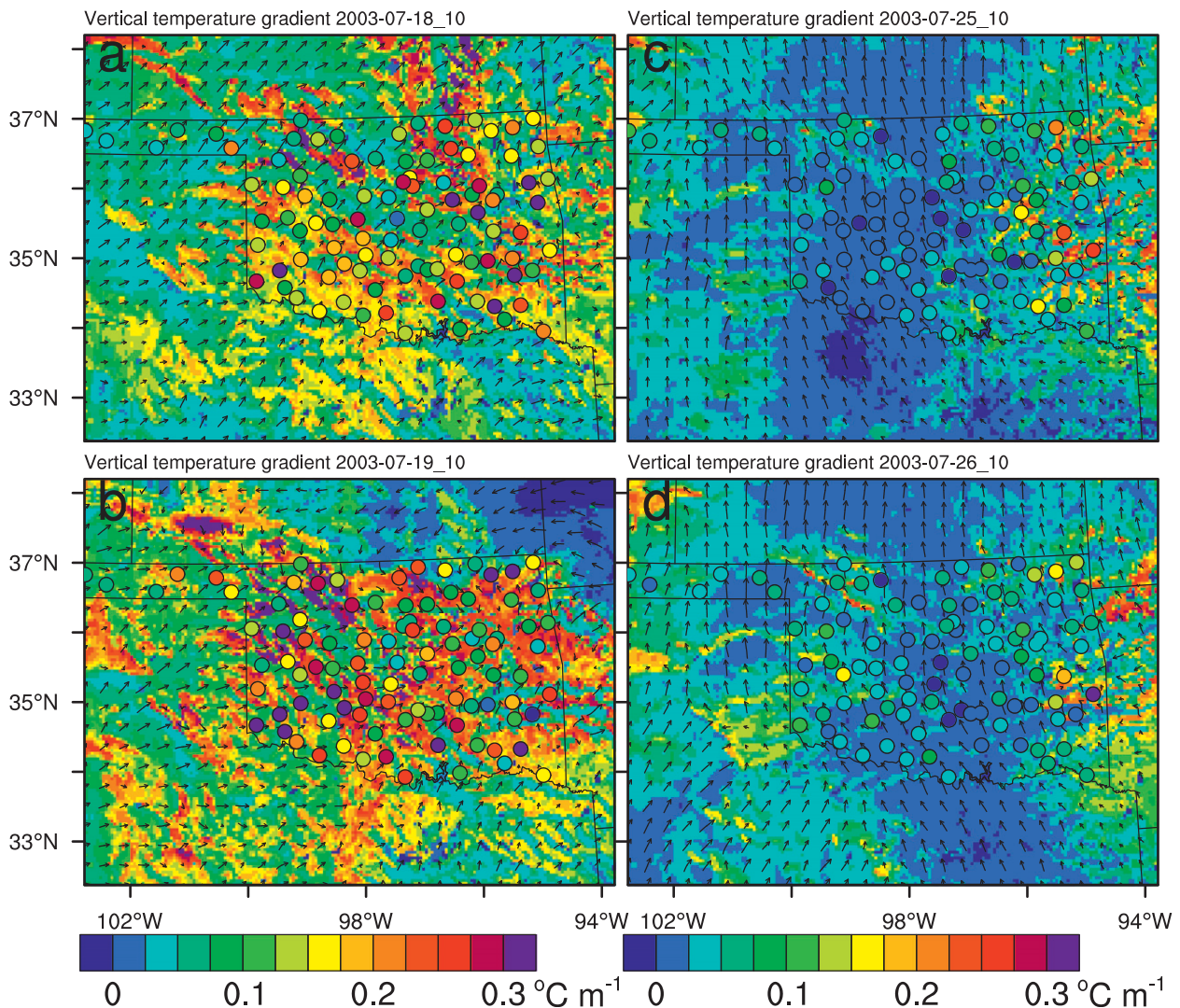


FIG. 12. Vertical temperature gradient dT/dz near the surface at 1000 UTC on the days with (a),(b) strong and (c),(d) weak UHIs. The simulated temperature gradient is computed from the simulated temperatures at 2 and ~ 12 m AGL. The observed gradient values at mesonet sites are indicated by shaded circles and are calculated from the observed temperatures at 1.5 and 9 m AGL.

improved representation of the urban canopy in the WRF simulations should investigate in more detail how urban areas affect both the dynamic and thermodynamic structures of the NBL, which is very important for air-quality studies.

As expected, the WRF simulations (Fig. 15) captured the observed (Fig. 4) diurnal variation of UHI intensity and the contrast between the strong- and weak-UHI episodes very well. The simulations further highlight that the diurnal variation of the rural PBL height (represented by the average PBL height at the six mesonet sites) modulates the diurnal variation of UHI intensity (Fig. 15). When the boundary layer collapsed during the early evening transition, UHI intensity increased abruptly, which is consistent with previously reported

strong increases in UHI intensities around the evening transition in cities such as Bucharest (Tumanov et al. 1999), Paris (Lemonsu and Masson 2002), and London (Bohnenstengel et al. 2011). When the boundary layer redeveloped rapidly on the following day, the UHI intensity decreased quickly (Fig. 15a). During the weak-UHI episode, the nighttime PBL heights (~ 400 – 600 m) were 3–4 times those during the strong-UHI episode (~ 100 – 200 m). Thus, boundary layer structure is important for UHI assessments.

A comparison of simulated skin temperatures (TSK) and land surface temperatures (LST) derived from the MODIS data is shown in Fig. 16. Given that the WRF model captures the external meteorological factors reasonably well (as discussed above), the WRF model

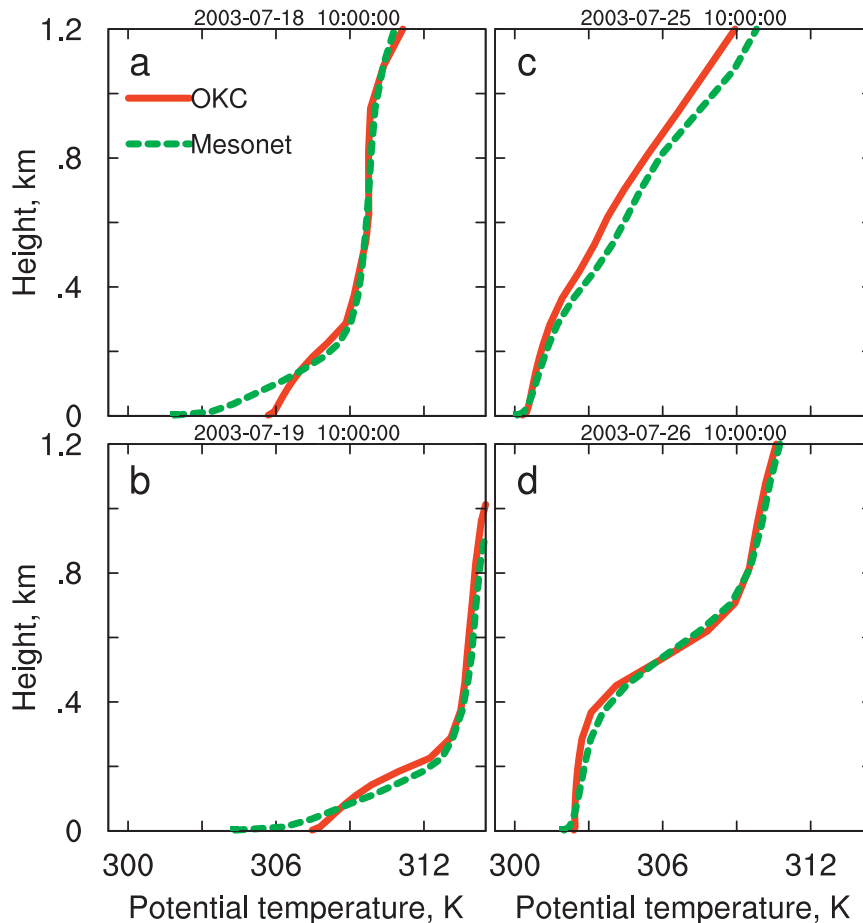


FIG. 13. Profiles of simulated potential temperature at 1000 UTC on the days with (a),(b) strong and (c),(d) weak UHIs. Red lines represent profiles extracted at the center of OKC, and green lines represent mean profiles at the six mesonet sites around OKC.

coupled with the single-layer UCM reproduces the MODIS-derived UHI intensities well. Both the model and MODIS data show the clear contrasts between urban and rural areas during the strong-UHI episode, and both show smeared-out contrasts during the weak-UHI episode. A negative bias of MODIS LST relative to WRF TSK (i.e., TSK is systematically higher than LST) can be noted, however, which may be due to the uncertainties in the MODIS data (Wan and Li 2008), model inputs (e.g., insufficient soil moisture; Hu et al. 2010), and model errors. The relationship between the satellite-derived LST and air/skin temperature remains the greatest unknown in remotely sensed studies of UHI (Voogt and Oke 2003; Fung et al. 2009; Nichol et al. 2009; Mohan et al. 2013).

The results presented so far have highlighted that the UHI intensity in Oklahoma City is correlated with the strength of the LLJ. Using two episodes, we could then demonstrate that this correlation appears to be related to the role of the LLJ in enhancing vertical mixing within

the NBL and in modulating the temperature inversion strength, primarily at rural sites. As a last step, we thus tested whether the temperature inversion observed near the surface at rural Oklahoma Mesonet sites can be used as a direct indicator of the UHI intensity. A time series and scatterplot between the average temperature inversion observed at the selected six rural mesonet sites (see Fig. 1b) and the OKC UHI intensity are shown in Fig. 17 for July of 2003. The daily variation of the UHI intensity follows the trends of the inversion strength, and the correlation between the two parameters was as high as 0.83. This result implies that temperature inversion in the surrounding rural area can be used as an indicator for UHI intensity. From statistical studies (e.g., Unger 1996; Unger et al. 2001; Fast et al. 2005; Morris et al. 2001), cloudiness was also reported to be another important factor in modulating UHI intensity; that is, the lower the cloudiness is, the stronger the UHI is, and the higher the cloudiness is, the weaker the UHI is. The

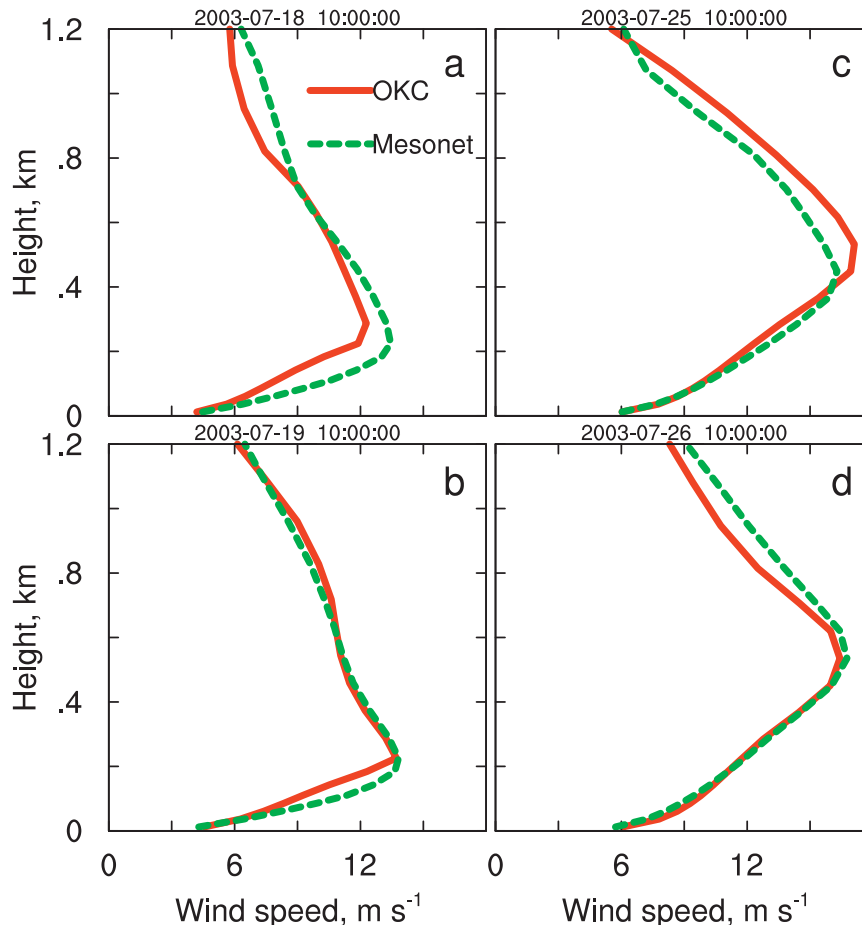


FIG. 14. As in Fig. 13, but for simulated vertical profiles of wind speed.

impact of cloudiness on UHI may also be related to the reduction of the stability near the surface (Fast et al. 2005; Verzijlbergh et al. 2009; Hu et al. 2011). Thus, temperature inversion as an indicator of UHI intensity may inherently account for the presence of cloud. The detailed mechanism through which cloudiness affects UHI is subject to further study, however.

4. Conclusions and discussion

The day-to-day nocturnal UHI intensity in OKC showed great variability in July of 2003. A significant correlation was found between the mean nocturnal UHI intensity and the strength of the nocturnal LLJ. During a weak-UHI episode, an east-to-west pressure gradient

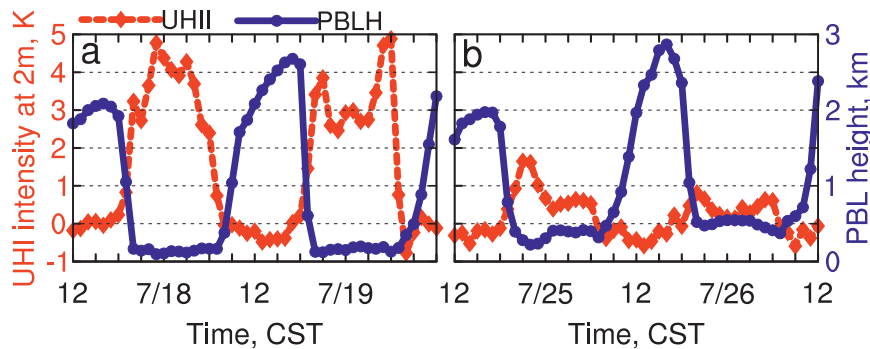


FIG. 15. Time series of simulated UHI intensity at 2 m and average PBL height at the six mesonet sites around OKC on the days with (a) strong and (b) weak UHIs.

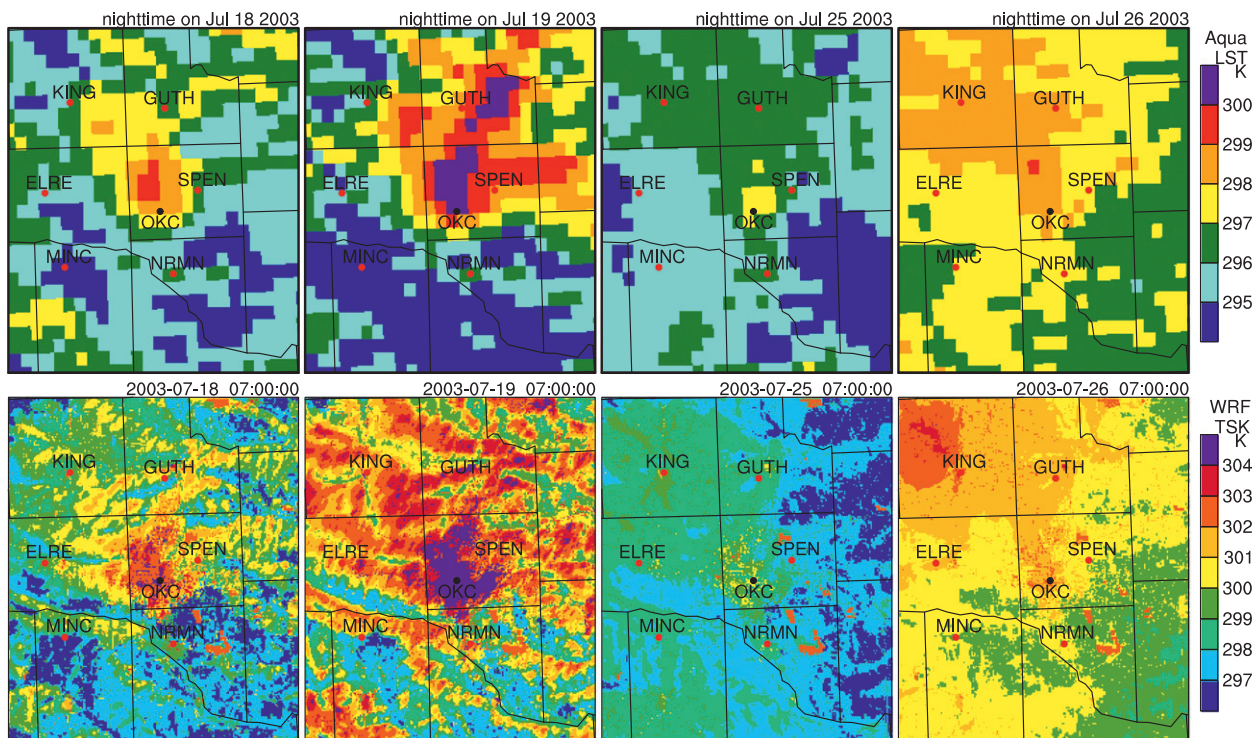


FIG. 16. Horizontal distribution of (top) LST retrieved from the *Aqua* MODIS data and (bottom) TSK simulated by WRF on (left to right) 18, 19, 25, and 26 July. The *Aqua* MODIS LST is at 0130 local time (nighttime overpass time), and the WRF TSK is at 0100 local time.

contributed to the acceleration of the northward-blowing LLJ over the Great Plains. During such nights, strong shear on the underside of the LLJ induced enhanced turbulent mixing, which resulted in a deeper and less stable NBL at the rural sites surrounding OKC. Under these conditions, urban effects, related to the hotter and rougher surface, did not strongly affect the temperature profiles, which explains the weak UHI signature. In contrast, on the nights with a weaker LLJ, a shallower stable boundary layer with stronger temperature inversions developed. In such cases, enhanced mixing in urban regions leads to pronounced urban-rural contrasts in the thermal structure of the NBL and accordingly much higher UHI intensities. In general, the UHI intensity declined quickly with height, and at ~ 100 m above the surface the urban air became cooler than the surrounding rural air.

Rural temperature inversion strength (i.e., vertical temperature gradient) near the surface is shown to be a direct indicator for nocturnal UHI intensity. In the cases studied, shear-induced turbulent mixing developing on the underside of LLJs modulated the near-surface temperature inversion at night. The day-to-day variation of nocturnal UHI intensity in OKC in July of 2003 could thus be explained by differences in the LLJ strength

caused by different synoptic conditions. In previous studies, synoptic conditions were also reported to influence UHI intensity (e.g., Unger 1996; Tumanov et al. 1999; Morris and Simmonds 2000; Mihalakakou et al. 2002), but the novelty of our study is that we could identify enhanced turbulent mixing triggered by LLJs as a mechanism by which synoptic conditions alter UHI intensity.

This paper emphasizes the importance of mesoscale meteorological factors (e.g., LLJs or stability in the stable boundary layer) in modulating the UHI intensity. To successfully capture such meteorological factors, a proper PBL scheme is necessary. The YSU scheme has been successfully applied in numerous studies for various purposes (e.g., Hu et al. 2010; Hong 2010; Mohan and Bhati 2011) and was initially tested in this study. The strength of LLJs was, however, underestimated when using the YSU PBL scheme because mechanical mixing during nighttime is overestimated (Storm et al. 2008; Hu et al. 2010, 2012; Shin and Hong 2011). Because of the unrealistic, strong mixing, the model underestimated the strength of the temperature inversions in the NBL, and, as a result, the skill in predicting UHI intensity was also poor when the YSU PBL scheme was selected. For the studied episodes, better results were obtained with the

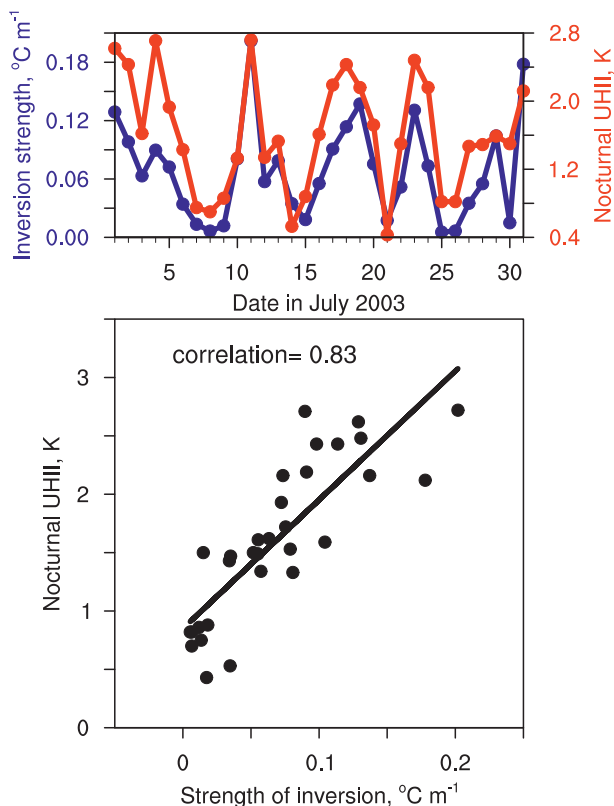


FIG. 17. (top) Time series of observed mean nocturnal UHI intensity at 9 m and inversion strength at the six mesonet sites, and (bottom) their correlation.

ACM2 PBL scheme in simulating nocturnal LLJs and their impacts on the UHI intensity. Nevertheless, modeling of the stably stratified atmospheric boundary layer remains a challenging task. A greater emphasis is needed on the improvement of the parameterization methods (Cuxart et al. 2006; Teixeira et al. 2008; Fernando and Weil 2010). To correctly predict UHI intensity and spatial extent, the model also needs to reasonably capture important effects of the urban canopy on the structure, dynamics, and turbulence of the NBL. In this study, a single-layer urban model coupled with the Noah land surface model appeared to be able to capture the urban effects on the atmospheric boundary layer (our earlier investigation using the Noah model alone for land surface treatment also captured the bulk effects of urban area to a certain extent). To study the interactions between the LLJ and UHI in more detail and to evaluate detailed UHI mitigation strategies, more-sophisticated urban canopy models are available and can be applied in future studies (Chen et al. 2011b; Bohnenstengel et al. 2011; Salamanca et al. 2011, 2012; Best and Grimmond 2012). Such studies will require detailed, simultaneous urban and rural observations of the dynamic and thermal

structures of the boundary layer to evaluate and further improve urban and boundary layer schemes.

In addition to affecting the UHI, LLJs may also have important implications for the transport and dispersion of pollutants (Banta et al. 1998; Hu et al. 2013). Hu et al. (2013) reported that strong turbulent mixing induced by nocturnal LLJs transported ozone-richer residual-layer air to the surface, where ozone was efficiently removed by chemical reactions and dry deposition, and, as a result, boundary layer ozone on the subsequent day was reduced. In an analysis of ozone concentrations observed at U.S. Environmental Protection Agency surface monitoring sites in the OKC metropolitan areas in July of 2003, isolated nocturnal secondary ozone maxima were also found during the nights with strong LLJs. More details about the impacts of LLJs on air quality are presented in Klein et al. (2013, manuscript submitted to *Bound.-Layer Meteor.*).

Acknowledgments. This work was supported by funding from the Office of the Vice President for Research at the University of Oklahoma. The second author was also supported through the NSF Career Award ILREUM (NSF ATM 0547882). The third author was also supported by NSF Grants OCI-0905040, AGS-0802888, AGS-0750790, AGS-0941491, AGS-1046171, and AGS-1046081. Computations were performed at the Texas Advanced Computing Center (TACC). Jeffrey B. Basara provided the two temperature datasets collected in OKC. Four anonymous reviewers provided helpful comments that improved the manuscript.

REFERENCES

- Acevedo, O. C., and D. R. Fitzjarrald, 2001: The early evening surface-layer transition: Temporal and spatial variability. *J. Atmos. Sci.*, **58**, 2650–2667.
- Allwine, K. J., M. J. Leach, L. W. Stockham, J. S. Shinn, R. P. Hosker, J. F. Bowers, and J. C. Pace, 2004: Overview of JOINT URBAN 2003—An atmospheric dispersion study in Oklahoma City. Preprints, *Symp. on Planning, Nowcasting, and Forecasting in the Urban Zone/Eighth Symp. on Integrated Observing and Assimilation Systems for Atmosphere, Oceans, and Land Surface*, Seattle, WA, Amer. Meteor. Soc., J7.1. [Available online at <https://ams.confex.com/ams/pdfpapers/74349.pdf>.]
- Alonso, M. S., M. R. Fidalgo, and J. L. Labajo, 2007: The urban heat island in Salamanca (Spain) and its relationship to meteorological parameters. *Climate Res.*, **34**, 39–46.
- Arnfield, A. J., 2003: Two decades of urban climate research: A review of turbulence, exchanges of energy and water, and the urban heat island. *Int. J. Climatol.*, **23**, 1–26.
- Balsley, B. B., G. Svensson, and M. Tjernstrom, 2008: On the scale-dependence of the gradient Richardson number in the residual layer. *Bound.-Layer Meteor.*, **127**, 57–72.

- Banta, R. M., and Coauthors, 1998: Daytime buildup and nighttime transport of urban ozone in the boundary layer during a stagnation episode. *J. Geophys. Res.*, **103**, 22 519–22 544.
- , R. K. Newsom, J. K. Lundquist, Y. L. Pichugina, R. L. Coulter, and L. Mahrt, 2002: Nocturnal low-level jet characteristics over Kansas during CASES-99. *Bound.-Layer Meteor.*, **105**, 221–252.
- , Y. L. Pichugina, and R. K. Newsom, 2003: Relationship between low-level jet properties and turbulence kinetic energy in the nocturnal stable boundary layer. *J. Atmos. Sci.*, **60**, 2549–2555.
- , —, and W. A. Brewer, 2006: Turbulent velocity-variance profiles in the stable boundary layer generated by a nocturnal low-level jet. *J. Atmos. Sci.*, **63**, 2700–2719.
- Basara, J. B., P. K. Hall Jr., A. J. Schroeder, B. G. Illston, and K. L. Nemunaitis, 2008: Diurnal cycle of the Oklahoma City urban heat island. *J. Geophys. Res.*, **113**, D20109, doi:10.1029/2008JD010311.
- Best, M. J., and C. S. B. Grimmond, 2012: Analysis of the seasonal cycle within the First International Urban Land-Surface Model Comparison. *Bound.-Layer Meteor.*, **146**, 421–446.
- Blackadar, A. K., 1957: Boundary-layer wind maxima and their significance for the growth of nocturnal inversions. *Bull. Amer. Meteor. Soc.*, **38**, 283–290.
- Bohnstengel, S. I., S. Evans, P. A. Clark, and S. E. Belcher, 2011: Simulations of the London urban heat island. *Quart. J. Roy. Meteor. Soc.*, **137**, 1625–1640.
- Bonner, W. D., 1968: Climatology of the low level jet. *Mon. Wea. Rev.*, **96**, 833–850.
- Bornstein, R. D., 1968: Observations of the urban heat island effect in New York City. *J. Appl. Meteor.*, **7**, 575–582.
- Brandsma, T., and D. Wolters, 2012: Measurement and statistical modeling of the urban heat island of the city of Utrecht (the Netherlands). *J. Appl. Meteor. Climatol.*, **51**, 1046–1060.
- Brown, M. J., A. Ivey, T. N. McPherson, D. Boswell, and E. R. Paradyjak, 2004: A study of the Oklahoma City urban heat island using ground measurements and remote sensing. Preprints, *Fifth Symp. on the Urban Environment*, Vancouver, BC, Canada, Amer. Meteor. Soc., 2.5A. [Available online at <https://ams.confex.com/ams/pdfpapers/80316.pdf>.]
- Burian, S., A. McKinnon, J. Hartman, and W. Han, 2005: National Building Statistics Database: Oklahoma City. Los Alamos National Laboratory Rep. LA-UR-05-8153, 17 pp.
- Camilloni, I., and M. Barrucand, 2012: Temporal variability of the Buenos Aires, Argentina, urban heat island. *Theor. Appl. Climatol.*, **107**, 47–58.
- Chen, F., and J. Dudhia, 2001: Coupling an advanced land surface–hydrology model with the Penn State–NCAR MM5 modeling system. Part I: Model implementation and sensitivity. *Mon. Wea. Rev.*, **129**, 569–585.
- , S. G. Miao, M. Tewari, J. W. Bao, and H. Kusaka, 2011a: A numerical study of interactions between surface forcing and sea breeze circulations and their effects on stagnation in the greater Houston area. *J. Geophys. Res.*, **116**, D12105, doi:10.1029/2010JD015533.
- , and Coauthors, 2011b: The integrated WRF/urban modeling system: Development, evaluation, and applications to urban environmental problems. *Int. J. Climatol.*, **31**, 273–288.
- Chow, W. T. L., D. Brennan, and A. J. Brazel, 2012: Urban heat island research in Phoenix, Arizona: Theoretical contributions and policy applications. *Bull. Amer. Meteor. Soc.*, **93**, 517–530.
- Cui, Y. Y., and B. de Foy, 2012: Seasonal variations of the urban heat island at the surface and the near-surface and reductions due to urban vegetation in Mexico City. *J. Appl. Meteor. Climatol.*, **51**, 855–868.
- Cuxart, J., and Coauthors, 2006: Single-column model inter-comparison for a stably stratified atmospheric boundary layer. *Bound.-Layer Meteor.*, **118**, 273–303.
- De Wekker, S. F. J., L. K. Berg, J. Allwine, J. C. Doran, and W. J. Shaw, 2004: Boundary-layer structure upwind and downwind of Oklahoma City during the Joint Urban 2003 field study. Preprints, *Fifth Conf. on Urban Environment*, Vancouver, BC, Canada, Amer. Meteor. Soc., 3.20. [Available online at <https://ams.confex.com/ams/pdfpapers/80355.pdf>.]
- Draxl, C., A. N. Hahmann, A. Peña, and G. Giebel, 2013: Evaluating winds and vertical wind shear from Weather Research and Forecasting model forecasts using seven planetary boundary layer schemes. *Wind Energy*, doi:10.1002/we.1555, in press.
- Dudhia, J., 1989: Numerical study of convection observed during the Winter Monsoon Experiment using a mesoscale two-dimensional model. *J. Atmos. Sci.*, **46**, 3077–3107.
- Fast, J. D., J. C. Torcolini, and R. Redman, 2005: Pseudovertical temperature profiles and the urban heat island measured by a temperature datalogger network in Phoenix, Arizona. *J. Appl. Meteor.*, **44**, 3–13.
- Fernando, H. J. S., and J. C. Weil, 2010: Whither the stable boundary layer? *Bull. Amer. Meteor. Soc.*, **91**, 1475–1484.
- Fiebrich, C. A., and K. C. Crawford, 2001: The impact of unique meteorological phenomena detected by the Oklahoma Mesonet and ARS Micronet on automated quality control. *Bull. Amer. Meteor. Soc.*, **82**, 2173–2187.
- Fischer, E. M., K. W. Oleson, and D. M. Lawrence, 2012: Contrasting urban and rural heat stress responses to climate change. *Geophys. Res. Lett.*, **39**, L03705, doi:10.1029/2011GL050576.
- Floors, R., C. L. Vincent, S. E. Gryning, A. Peña, and E. Batchvarova, 2013: The wind profile in the coastal boundary layer: Wind lidar measurements and numerical modelling. *Bound.-Layer Meteor.*, **147**, 469–491.
- Fung, W. Y., K. S. Lam, J. Nichol, and M. S. Wong, 2009: Derivation of nighttime urban air temperatures using a satellite thermal image. *J. Appl. Meteor. Climatol.*, **48**, 863–872.
- Gedzelman, S. D., S. Austin, R. Cermak, N. Stefano, S. Partridge, S. Quesenberry, and D. A. Robinson, 2003: Mesoscale aspects of the urban heat island around New York City. *Theor. Appl. Climatol.*, **75**, 29–42.
- Georgakis, C., M. Santamouris, and G. Kaisarli, 2010: The vertical stratification of air temperature in the center of Athens. *J. Appl. Meteor. Climatol.*, **49**, 1219–1232.
- Goldreich, Y., 2006: Ground and top of canopy layer urban heat island partitioning on an airborne image. *Remote Sens. Environ.*, **104**, 247–255.
- Grimmond, C. S. B., 2007: Urbanization and global environmental change: Local effects of urban warming. *Geogr. J.*, **173**, 83–88.
- , H.-B. Su, B. Offerle, B. Crawford, S. Scott, S. Zhong, and C. Clements, 2004: Variability of sensible heat fluxes in a suburban area of Oklahoma City. Preprints, *Symp. on Planning, Nowcasting, and Forecasting in the Urban Zone/Eighth Symp. on Integrated Observing and Assimilation Systems for Atmosphere, Oceans, and Land Surface*, Seattle, WA, Amer. Meteor. Soc., J7.2. [Available online at <https://ams.confex.com/ams/pdfpapers/67542.pdf>.]

- He, H., and F. Zhang, 2010: Diurnal variations of warm-season precipitation over north China. *Mon. Wea. Rev.*, **138**, 1017–1025.
- Hidalgo, J., V. Masson, A. Baklanov, G. Pigeon, and L. Gimeno, 2008: Advances in urban climate modeling. *Ann. N.Y. Acad. Sci.*, **1146**, 354–374.
- Higgins, R. W., Y. Yao, E. S. Yarosh, J. E. Janowiak, and K. C. Mo, 1997: Influence of the Great Plains low-level jet on summertime precipitation and moisture transport over the central United States. *J. Climate*, **10**, 481–507.
- Hoecker, W. H., 1963: Three southerly low-level jet systems delineated by the Weather Bureau special pibal network of 1961. *Mon. Wea. Rev.*, **91**, 573–582.
- Holton, J. R., 1967: The diurnal boundary layer wind oscillation above sloping terrain. *Tellus*, **19**, 199–205.
- Hong, S.-Y., 2010: A new stable boundary-layer mixing scheme and its impact on the simulated East Asian summer monsoon. *Quart. J. Roy. Meteor. Soc.*, **136**, 1481–1496.
- , J. Dudhia, and S.-H. Chen, 2004: A revised approach to ice microphysical processes for the bulk parameterization of cloud and precipitation. *Mon. Wea. Rev.*, **132**, 103–120.
- , Y. Noh, and J. Dudhia, 2006: A new vertical diffusion package with explicit treatment of entrainment processes. *Mon. Wea. Rev.*, **134**, 2318–2341.
- Hu, X.-M., J. W. Nielsen-Gammon, and F. Zhang, 2010: Evaluation of three planetary boundary layer schemes in the WRF model. *J. Appl. Meteor. Climatol.*, **49**, 1831–1844.
- , F. Q. Zhang, G. Yu, J. D. Fuentes, and L. T. Wu, 2011: Contribution of mixed-phase boundary layer clouds to the termination of ozone depletion events in the Arctic. *Geophys. Res. Lett.*, **38**, L21801, doi:10.1029/2011GL049229.
- , D. C. Doughty, K. J. Sanchez, E. Joseph, and J. D. Fuentes, 2012: Ozone variability in the atmospheric boundary layer in Maryland and its implications for vertical transport model. *Atmos. Environ.*, **46**, 354–364.
- , P. Klein, M. Xue, F. Zhang, D. C. Doughty, R. Forkel, E. Joseph, and J. D. Fuentes, 2013: Impact of the vertical mixing induced by low-level jets on boundary layer ozone concentration. *Atmos. Environ.*, **70**, 123–130.
- Hunt, E. D., J. B. Basara, and C. R. Morgan, 2007: Significant inversions and rapid in situ cooling at a well-sited Oklahoma Mesonet station. *J. Appl. Meteor. Climatol.*, **46**, 353–367.
- Jiang, X. Y., C. Wiedinmyer, F. Chen, Z. L. Yang, and J. C. F. Lo, 2008: Predicted impacts of climate and land use change on surface ozone in the Houston, Texas, area. *J. Geophys. Res.*, **113**, D20312, doi:10.1029/2008JD009820.
- Kallistratova, M. A., and R. D. Kouznetsov, 2012: Low-level jets in the Moscow region in summer and winter observed with a sodar network. *Bound.-Layer Meteor.*, **143**, 159–175.
- Klein, P. M., J. K. Lundquist, and J. B. Basara, 2010: Mixing processes in the nocturnal atmospheric boundary layer and their impacts on urban ozone concentrations and heat island intensity. Preprints, *19th Symp. on Boundary Layers and Turbulence/29th Conf. on Agricultural and Forest Meteorology/9th Symp. on the Urban Environment*, Keystone, CO, Amer. Meteor. Soc., J2.2. [Available online at <https://ams.confex.com/ams/pdfpapers/173200.pdf>.]
- Kolling, J. S., J. E. Pleim, H. E. Jeffries, and W. Vizuete, 2012: A multisensor evaluation of the Asymmetric Convective Model, version 2, in southeast Texas. *J. Air Waste Manage.*, **63**, 41–53.
- Kusaka, H., H. Kondo, Y. Kikegawa, and F. Kimura, 2001: A simple single-layer urban canopy model for atmospheric models: Comparison with multi-layer and slab models. *Bound.-Layer Meteor.*, **101**, 329–358.
- Lemonsu, A., and V. Masson, 2002: Simulation of a summer urban breeze over Paris. *Bound.-Layer Meteor.*, **104**, 463–490.
- Lin, C. Y., F. Chen, J. C. Huang, W. C. Chen, Y. A. Liou, W. N. Chen, and S. C. Liu, 2008: Urban heat island effect and its impact on boundary layer development and land–sea circulation over northern Taiwan. *Atmos. Environ.*, **42**, 5635–5649.
- Liu, Y., F. Chen, T. Warner, and J. Basara, 2006: Verification of a mesoscale data-assimilation and forecasting system for the Oklahoma City area during the Joint Urban 2003 Field Project. *J. Appl. Meteor. Climatol.*, **45**, 912–929.
- Loughner, C. P., D. J. Allen, D.-L. Zhang, K. E. Pickering, R. R. Dickerson, and L. Landry, 2012: Roles of urban tree canopy and buildings in urban heat island effects: Parameterization and preliminary results. *J. Appl. Meteor. Climatol.*, **51**, 1775–1793.
- Lundquist, J. K., and J. D. Mirocha, 2008: Interaction of nocturnal low-level jets with urban geometries as seen in Joint Urban 2003 data. *J. Appl. Meteor. Climatol.*, **47**, 44–58.
- Mahrt, L., and D. Vickers, 2002: Contrasting vertical structures of nocturnal boundary layers. *Bound.-Layer Meteor.*, **105**, 351–363.
- McPherson, R. A., and Coauthors, 2007: Statewide monitoring of the mesoscale environment: A technical update on the Oklahoma Mesonet. *J. Atmos. Oceanic Technol.*, **24**, 301–321.
- Miao, S. G., and F. Chen, 2008: Formation of horizontal convective rolls in urban areas. *Atmos. Res.*, **89**, 298–304.
- , and Coauthors, 2009: An observational and modeling study of characteristics of urban heat island and boundary layer structures in Beijing. *J. Appl. Meteor. Climatol.*, **48**, 484–501.
- , F. Chen, Q. C. Li, and S. Y. Fan, 2011: Impacts of urban processes and urbanization on summer precipitation: A case study of heavy rainfall in Beijing on 1 August 2006. *J. Appl. Meteor. Climatol.*, **50**, 806–825.
- Mihalakakou, P., H. A. Flocas, M. Santamouris, and C. G. Helmis, 2002: Application of neural networks to the simulation of the heat island over Athens, Greece, using synoptic types as a predictor. *J. Appl. Meteor.*, **41**, 519–527.
- Mlawer, E. J., S. J. Taubman, P. D. Brown, M. J. Iacono, and S. A. Clough, 1997: Radiative transfer for inhomogeneous atmospheres: RRTM, a validated correlated-*k* model for the longwave. *J. Geophys. Res.*, **102**, 16 663–16 682.
- Mohan, M., and S. Bhati, 2011: Analysis of WRF model performance over subtropical region of Delhi, India. *Adv. Meteor.*, 621235, doi:10.1155/2011/621235.
- , Y. Kikegawa, B. R. Gurjar, S. Bhati, A. Kandya, and K. Ogawa, 2012: Urban heat island assessment for a tropical urban airshed in India. *Atmos. Climate Sci.*, **2**, 127–138.
- , —, —, —, and N. Kolli, 2013: Assessment of urban heat island effect for different land use–land cover from micrometeorological measurements and remote sensing data for megacity Delhi. *Theor. Appl. Climatol.*, **112**, 647–658.
- Morris, C. J. G., and I. Simmonds, 2000: Associations between varying magnitudes of the urban heat island and the synoptic climatology in Melbourne, Australia. *Int. J. Climatol.*, **20**, 1931–1954.
- , —, and N. Plummer, 2001: Quantification of the influences of wind and cloud on the nocturnal urban heat island of a large city. *J. Appl. Meteor.*, **40**, 169–182.

- Nichol, J. E., W. Y. Fung, K. S. Lam, and M. S. Wong, 2009: Urban heat island diagnosis using ASTER satellite images and “in situ” air temperature. *Atmos. Res.*, **94**, 276–284.
- Oke, T. R., 1976: The distinction between canopy and boundary-layer urban heat islands. *Atmosphere*, **14**, 268–277.
- , 1981: Canyon geometry and the nocturnal urban heat island: Comparison of scale model and field observations. *J. Climatol.*, **1**, 237–254.
- , 1982: The energetic basis of the urban heat island. *Quart. J. Roy. Meteor. Soc.*, **108**, 1–24.
- , D. G. Johnson, D. G. Steyn, and I. D. Watson, 1991: Simulation of surface urban heat islands under “ideal” conditions at night—Part 2: Diagnosis of causation. *Bound.-Layer Meteor.*, **56**, 339–358.
- Parish, T. R., and L. D. Oolman, 2010: On the role of sloping terrain in the forcing of the Great Plains low-level jet. *J. Atmos. Sci.*, **67**, 2690–2699.
- Pleim, J. E., 2007a: A combined local and nonlocal closure model for the atmospheric boundary layer. Part I: Model description and testing. *J. Appl. Meteor. Climatol.*, **46**, 1383–1395.
- , 2007b: A combined local and nonlocal closure model for the atmospheric boundary layer. Part II: Application and evaluation in a mesoscale meteorological model. *J. Appl. Meteor. Climatol.*, **46**, 1396–1409.
- Poulos, G. S., and Coauthors, 2002: CASES-99: A comprehensive investigation of the stable nocturnal boundary layer. *Bull. Amer. Meteor. Soc.*, **83**, 555–581.
- Rizwan, A. M., L. Y. C. Dennis, and C. Liu, 2008: A review on the generation, determination and mitigation of urban heat island. *J. Environ. Sci.*, **20**, 120–128.
- Runnalls, K. E., and T. R. Oke, 1998: The urban heat island of Vancouver, BC. Preprints, *Second Symp. on the Urban Environment*, Albuquerque, NM, Amer. Meteor. Soc., 84–87.
- Ryan, W. F., 2004: The low-level jet in Maryland: Profiler observations and preliminary climatology. Maryland Dept. of the Environment Rep., 43 pp. [Available online at http://www.mde.state.md.us/assets/document/AirQuality/BALT_OZONE_SIP/Appendix_G5.pdf.]
- Ryu, Y.-H., and J.-J. Baik, 2012: Quantitative analysis of factors contributing to urban heat island intensity. *J. Appl. Meteor. Climatol.*, **51**, 842–854.
- Salamanca, F., A. Martilli, M. Tewari, and F. Chen, 2011: A study of the urban boundary layer using different urban parameterizations and high-resolution urban canopy parameters with WRF. *J. Appl. Meteor. Climatol.*, **50**, 1107–1128.
- , —, and C. Yague, 2012: A numerical study of the urban heat island over Madrid during the DESIREX (2008) campaign with WRF and an evaluation of simple mitigation strategies. *Int. J. Climatol.*, **32**, 2372–2386.
- Shahgedanova, M., T. P. Burt, and T. D. Davies, 1997: Some aspects of the three-dimensional heat island in Moscow. *Int. J. Climatol.*, **17**, 1451–1465.
- Shapiro, A., and E. Fedorovich, 2009: Nocturnal low-level jet over a shallow slope. *Acta Geophys.*, **57**, 950–980.
- , and —, 2010: Analytical description of a nocturnal low-level jet. *Quart. J. Roy. Meteor. Soc.*, **136**, 1255–1262.
- Shin, H. H., and S.-Y. Hong, 2011: Intercomparison of planetary boundary-layer parameterizations in the WRF model for a single day from CASES-99. *Bound.-Layer Meteor.*, **139**, 261–281.
- Skamarock, W. C., and Coauthors, 2008: A description of the Advanced Research WRF version 3. NCAR Tech. Note TN-475-STR, 113 pp.
- Song, J., K. Liao, R. L. Coulter, and B. M. Lesht, 2005: Climatology of the low-level jet at the Southern Great Plains Atmospheric Boundary Layer Experiments site. *J. Appl. Meteor.*, **44**, 1593–1606.
- Souch, C., and S. Grimmond, 2006: Applied climatology: Urban climate. *Prog. Phys. Geogr.*, **30**, 270–279.
- Steenefeld, G. J., S. Koopmans, B. G. Heusinkveld, L. W. A. van Hove, and A. A. M. Holtslag, 2011: Quantifying urban heat island effects and human comfort for cities of variable size and urban morphology in the Netherlands. *J. Geophys. Res.*, **116**, D20129, doi:10.1029/2011JD015988.
- Stewart, I. D., 2011: A systematic review and scientific critique of methodology in modern urban heat island literature. *Int. J. Climatol.*, **31**, 200–217.
- , and T. R. Oke, 2012: Local climate zones for urban temperature studies. *Bull. Amer. Meteor. Soc.*, **93**, 1879–1900.
- Storm, B., J. Dudhia, S. Basu, A. Swift, and I. Giammanco, 2008: Evaluation of the Weather Research and Forecasting Model on forecasting low-level jets: Implications for wind energy. *Wind Energy*, **12**, 81–90.
- Stull, R. B., 1988: *An Introduction to Boundary Layer Meteorology*. Kluwer, 666 pp.
- Sun, J., and F. Zhang, 2012: Impacts of mountain-plains solenoid on diurnal variations of rainfalls along the mei-yu front over east China plains. *Mon. Wea. Rev.*, **140**, 379–397.
- Teixeira, J., and Coauthors, 2008: Parameterization of the atmospheric boundary layer: A view from just above the inversion. *Bull. Amer. Meteor. Soc.*, **89**, 453–458.
- Ting, M., and H. Wang, 2006: The role of the North American topography on the maintenance of the Great Plains summer low-level jet. *J. Atmos. Sci.*, **63**, 1056–1068.
- Tumanov, S., A. Stan-Sion, A. Lupu, C. Soci, and C. Oprea, 1999: Influences of the city of Bucharest on weather and climate parameters. *Atmos. Environ.*, **33**, 4173–4183.
- Unger, J., 1996: Heat island intensity with different meteorological conditions in a medium-sized town: Szeged, Hungary. *Theor. Appl. Climatol.*, **54**, 147–151.
- , Z. Sumeghy, and J. Zoboki, 2001: Temperature cross-section features in an urban area. *Atmos. Res.*, **58**, 117–127.
- Verzijlbergh, R. A., H. J. J. Jonker, T. Heus, and J. V. G. de Arellano, 2009: Turbulent dispersion in cloud-topped boundary layers. *Atmos. Chem. Phys.*, **9**, 1289–1302.
- Voogt, J. A., and T. R. Oke, 2003: Thermal remote sensing of urban climates. *Remote Sens. Environ.*, **86**, 370–384.
- Wan, Z., and Z. L. Li, 2008: Radiance-based validation of the V5 MODIS land-surface temperature product. *Int. J. Remote Sens.*, **29**, 5373–5395.
- Wang, X. M., F. Chen, Z. Y. Wu, M. G. Zhang, M. Tewari, A. Guenther, and C. Wiedinmyer, 2009: Impacts of weather conditions modified by urban expansion on surface ozone: Comparison between the Pearl River delta and Yangtze River delta regions. *Adv. Atmos. Sci.*, **26**, 962–972.
- Wang, Y., C. L. Klipp, D. M. Garvey, D. A. Ligon, C. C. Williamson, S. S. Chang, R. K. Newsom, and R. Calhoun, 2007: Nocturnal low-level-jet-dominated atmospheric boundary layer observed by a Doppler lidar over Oklahoma City during JU2003. *J. Appl. Meteor. Climatol.*, **46**, 2098–2109.
- Wexler, H., 1961: A boundary layer interpretation of the low-level jet. *Tellus*, **13**, 368–378.
- Whiteman, C. D., X. D. Bian, and S. Y. Zhong, 1997: Low-level jet climatology from enhanced rawinsonde observations at a site in the southern Great Plains. *J. Appl. Meteor.*, **36**, 1363–1376.

- , J. M. Hubbe, and W. J. Shaw, 2000: Evaluation of an inexpensive temperature datalogger for meteorological applications. *J. Atmos. Oceanic Technol.*, **17**, 77–81.
- Xie, B., J. C.-H. Fung, A. Chan, and A. K.-H. Lau, 2012: Evaluation of nonlocal and local planetary boundary layer schemes in the WRF model. *J. Geophys. Res.*, **117**, D12103, doi:10.1029/2011JD017080.
- Zhang, D.-L., S. Zhang, and S. J. Weaver, 2006: Low-level jets over the mid-Atlantic states: Warm-season climatology and a case study. *J. Appl. Meteor. Climatol.*, **45**, 194–209.
- , Y.-X. Shou, and R. R. Dickerson, 2009: Upstream urbanization exacerbates urban heat island effects. *Geophys. Res. Lett.*, **36**, L24401, doi:10.1029/2009GL041082.
- Zhang, F., N. Bei, J. W. Nielsen-Gammon, G. Li, R. Zhang, A. Stuart, and A. Aksoy, 2007: Impacts of meteorological uncertainties on ozone pollution predictability estimated through meteorological and photochemical ensemble forecasts. *J. Geophys. Res.*, **112**, D04304, doi:10.1029/2006JD007429.
- Zhong, S., J. D. Fast, and X. Bian, 1996: A case study of the Great Plains low-level jet using wind profiler network data and a high-resolution mesoscale model. *Mon. Wea. Rev.*, **124**, 785–806.
- Zhou, Y., and J. M. Shepherd, 2010: Atlanta's urban heat island under extreme heat conditions and potential mitigation strategies. *Nat. Hazards*, **52**, 639–668.